IEEE Access
Multidisciplinary | Rapid Review | Open Access Journal

Received June 4, 2020, accepted June 23, 2020, date of publication June 25, 2020, date of current version July 7, 2020.

Digital Object Identifier 10.1109/ACCESS.2020.3005038

Modeling and Classification of Stator Inter-Turn Fault and Demagnetization Effects in BLDC Motor Using Rotor Back-EMF and Radial Magnetic Flux Analysis

ADIL USMAN, (Senior Member, IEEE), AND BHARAT SINGH RAJPUROHIT, (Senior Member, IEEE)
School of Computing and Electrical Engineering, Indian Institute of Technology Mandi, Mandi 175075, India

Corresponding author: Adil Usman (adilusman@ieee.org)

This work was supported in part by the Ministry of Electronics and Information Technology (MeitY).

ABSTRACT This paper shall carry out unique study and investigation on the individual and combined effect of Stator Inter-turn Fault (SITF) and rotor demagnetization effects in a Surface Mounted Permanent Magnet (SPM)-type Brushless Direct Current (BLDC) motor. Comprehensive modeling of fault is accomplished using the well-established fault modeling techniques such as Electrical Equivalent Circuit (EEC), Magnetic Equivalent Circuit (MEC), Numerical Methods (NMs) and hybrid modeling-based approaches. The extensive study of SITF conditions using an Improved Winding Function Theory (IWFT) gives better analysis to winding inductance L_S, under fault conditions, while modeling the demagnetization effects using MEC and NM based approaches gives more realistic magnetic field quantities. The outcomes obtained are further remodeled in the developed hybrid model of a BLDC motor to study the steady state performance of a machine in terms of rotor back-EMF, E_B and radial magnetic flux density B_g. The characteristic performance accomplished through the hybrid model system possess better accuracy with less computational time and therefore finds suitability among efficient and fast diagnosis technique feasible for industrial applications. The significant detectable changes in E_B and B_g under subjected fault conditions, assist in detection, identification and classification of faults in BLDC motor. By obtaining the similar outcome experimentally and under the load conditions, the proposed study on the classification of fault is validated.

INDEX TERMS Brushless direct current (BLDC) motors, demagnetization, electrical equivalent circuit (EEC), finite element (FE) method, improved winding function theory (IWFT), numerical methods (NMs), permanent magnet (PM), Simplorer, stator inter-turn fault (SITF), surface mounted PM (SPM).

I. INTRODUCTION

Surface Mounted Permanent Magnet (SPM)-type BLDC motor is widely used for high performance speed drive applications. Due to fast dynamic response, better efficiency and high torque density, SPM-type BLDC motors are more preferable in Electric Vehicles (EVs) and high precision-controlled operations [1]. However, during the continuous operation of a BLDC motor in industries, they are subjected to unfavorable environmental conditions resulting in the emergence of fault [2]. Faults in BLDC motors can be either on the stator or on the rotor of a machine. Condition monitoring thus becomes vital in diagnosing the fault in its incipient state in order to avoid the prolonged failure of the complete system under subjected conditions. It has been earlier reported in [3] about the classification and modeling of faults related to the PM motors and further concluded on the methods to be adopted for different types of fault conditions. Conventional fault modeling methods such as Electrical Equivalent Circuit (EEC), Magnetic Equivalent Circuit (MEC) and Numerical Method (NM) based approaches are more prominently used for the diagnosis of faults in PM synchronous machines [4]–[6].

During fault conditions, BLDC motor is persistent to Stator Winding Faults (SWFs) on the stator and demagnetization fault in the rotor of a machine [7], [8].

The associate editor coordinating the review of this manuscript and approving it for publication was Ruqiang Yan.

Among different demagnetization faults reported in literature [9]–[11], the rotor faults caused through the physical defect in PMs is widely encountered and diagnosed using the magnetic flux signatures [9]. However, the other type of rotor related faults like rotor eccentricity and imbalance has been diagnosed using Hall Effect (HE) field measurements [10]. Similarly, uniform demagnetization of rotor PMs is diagnosed using current and magnetic flux linkage-based analysis in [11]. For the Stator Inter-turn Fault (SITF) diagnosis, different machine quantities like stator winding currents (I_s) and motor back-EMF (E_B) are used as fault signatures for diagnosis [7], [12]. The approach deployed in modeling of winding related faults is preferably EEC and NMs based techniques [12], [13]. However, the fault diagnostic methods adopted are collectively model-based strategy and signal processing-based techniques. The advanced research findings as reported in [14], analyze the severity estimation of SITF faults in PMSM considering the residual voltages and current. It is thus comprehensible from the literature which explores on the individual machine fault diagnosis but fails to report the combined effect of faults eventuating at the same time in a machine. The proposed research shall therefore study the individual as well as the combined effect of stator and rotor related faults in a BLDC motor drive. The SITF conditions are modeled under stator winding related faults while the demagnetization of rotor PMs are analyzed for the rotor side fault conditions under steady state performance of a machine.

The Stator Inter-Turn Fault conditions under study are modeled analytically (EEC based methods) using Improved Winding Function Theory (IWFT) [15], [16] to achieve stator winding inductance L_S under subjected conditions. While the rotor demagnetization faults are modelled using the MEC [17], [18] and NM based approach to study the characteristics of rotor magnetic fields, B_g. The radial airgap magnetic field B_g and stator winding inductance L_S, are then remodeled in the EEC based model to develop an advance hybrid BLDC motor system. The proposed model accomplishes more realistic characteristics performance of the machine in terms of electromagnetic quantities like stator phase currents (I_s), motor back-EMF (E_B), and airgap magnetic flux (B_g), under subjected fault conditions. The combined effect of fault conditions is further analysed using the proposed modeling approach, in addition to validating the outcomes numerically.

The fault affected changes encountered in the rotor back-EMF, E_B and airgap magnetic field, B_g are analysed to classify the machine faults. A BLDC motor drive-testbed employing a FPGA based controller, is developed for carrying out the experimental investigations and study the performance of a machine under subjected individual and combined fault effects. Similar outcomes when obtained experimentally, validates the proposed research findings on the modeling and classification of faults. In addition, the outcomes obtained from the proposed modeling techniques are compared to draw an *accuracy-computational time-based* inference to be adopted by the industries for the expeditious diagnosis of machine faults. The faults are diagnosed in its incipient stage and prevent the prolonged failure of the complete system from shutdown.

The organization of paper is as follows. Section-II-III models the SPM-type BLDC motor under healthy, SITF, demagnetization fault conditions using EEC, MEC and NM based approach. Section IV develops a hybrid motor system to model the combined effect of both the faults. Section-V summarizes the harmonic analysis of motor under healthy and fault conditions while Section-VI gives experimental validation to the proposed fault modeling techniques. Section VII gives the deductions and classification to faults, and Section VIII illustrates the accuracy-computational time-based analysis for fault modeling approaches. Section IX studies the machine faults under load conditions.

II. MODELING OF STATOR INTER-TURN FAULT (SITF)

A. IMPROVED WINDING FUNCTION THEORY (IWFT) AND ELECTRICAL EQUIVALENT CIRCUIT (EEC) BASED ANALYSIS

The Electrical Equivalent Circuit (EEC) based model of a BLDC motor is developed, using the mathematical modeling equations referred in [1], [2]. However, the modeling equations related to motor back-EMF and rotor magnetic fields are given from (1)-(4).

$$v_s = R_s i_{s,a} + (L - M)\left(\frac{di_{s,a}}{dt}\right) + \left(\frac{d\lambda_{PM,s,a}}{dt}\right) \tag{1}$$

v_s is the motor supply phase voltage, $i_{s,a}$ is the stator phase current for phase A, $\lambda_{PM,s,a}$ is the flux linkage of a PM for phase A given in terms of back-EMF given in (2),

$$\left(\frac{d\lambda_{PM,s,a}}{dt}\right) = e_a, \quad \text{for Phase A} \tag{2}$$

$$e_a = \frac{K_e}{2}\omega_m F(\theta_e), \quad \text{for phase A} \tag{3}$$

where θ_e is an electrical angle of rotor, ω_m is the mechanical speed and $F(\theta_e)$ is a back–EMF or magnetic flux density reference function given in (4),

$$F(\theta_e) = \begin{cases} 1 & 0 \le \theta_e < \dfrac{2\pi}{3} \\ 1 - \dfrac{6}{\pi}\left(\theta_e - \dfrac{2\pi}{3}\right) & \dfrac{2\pi}{3} \le \theta_e < \pi \\ -1 & \pi \le \theta_e < \dfrac{5\pi}{3} \\ -1 + \dfrac{6}{\pi}\left(\theta_e - \dfrac{2\pi}{3}\right) & \dfrac{5\pi}{3} \le \theta_e < 2\pi \end{cases} \tag{4}$$

$L - M$ in (1) is referred as L_S where, L is a self-inductance while M is the mutual inductance between two windings. The inductance L_S can be calculated based on the winding distribution of a machine given in Fig. 1. In the proposed research, L_S is modeled using Improved Winding Function Theory (IWFT) which is given through mathematical equation from (5)-(8).

$$L_{AB}(\theta_m) = \frac{\mu_0 . r . l}{g_a} \int_0^{2\pi} N_A(\phi) . N_B(\phi)\, d\phi \tag{5}$$

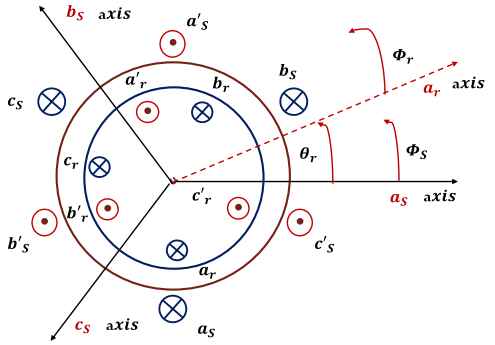

FIGURE 1. Stator winding arrangement for SPM-type BLDC motor.

where $N_A(\phi)$ and $N_B(\phi)$ are the winding functions of phase A and phase B respectively. While the self-inductance of a winding is given in (6) as,

$$L_{AA}(\theta_m) = \frac{\mu_0 . r . l}{g_a} \int_0^{2\pi} N_A^2(\phi)\, d\phi \tag{6}$$

Using (5)-(6), the stator inductance (L_s) can be obtained under healthy conditions, as given in (7).

$$[L_s] = \begin{bmatrix} L_{AA} & L_{AB} & L_{AC} \\ L_{BA} & L_{BB} & L_{BC} \\ L_{CA} & L_{CB} & L_{CC} \end{bmatrix} \tag{7}$$

where L_{AA}, L_{BB}, and L_{CC} are the self-inductances while L_{AB}, L_{AC}, L_{BA}, L_{BC}, L_{CA}, and L_{CB} are the mutual inductances.

Further, the permeability of free space, $\mu_0 = 4\pi * 10^{-7}$ N/A^2 (or H/m), radius of the rotor, $r = 3.94$ cm, the rotor length, $l = 5.00$ cm, while the airgap length, $g_a = 0.53$ cm. Substituting the geometrical values in (8), the total winding inductance can be calculated which is found to be $L = 0.136$ mH as also shown in Fig. 2.

$$L = \frac{\mu_0 . r . l}{g_a} N^2 \frac{\pi}{64} \tag{8}$$

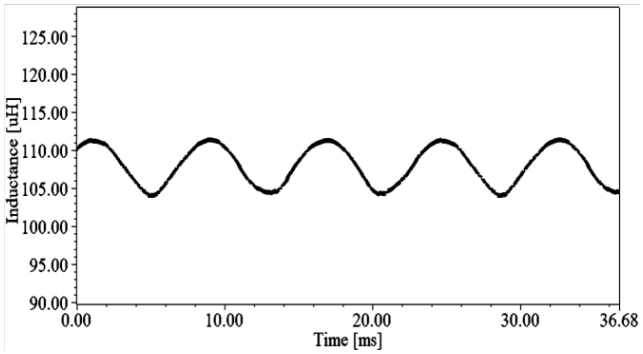

FIGURE 2. Stator winding inductance Ls = 136 uH or 0.136 mH.

The closed loop model of an analytical BLDC motor is developed using the estimated L_s parameter, while the other machine parameters are referred from Table-1. The equivalent block diagram of a motor drive operating under 120-degree conduction operation is given through Fig. 3.

TABLE 1. Analytical parameters of a BLDC motor.

Symbol	Parameters	Value
P_o	Output Power	850 W
V	Supply Voltage	48 VDC
P_W	Windage Loss	20 W
ω	Rated Speed	277.50 rad/s
I	Rated Current	21 A
T_e	Rated Torque	3.06 N-m
φ	No. of Phases	3
η	Efficiency	85 %
p	No. of poles	8
n_s	No. of slots	12
n_t	Turns per phase	24
n_c	Turns per coil	6

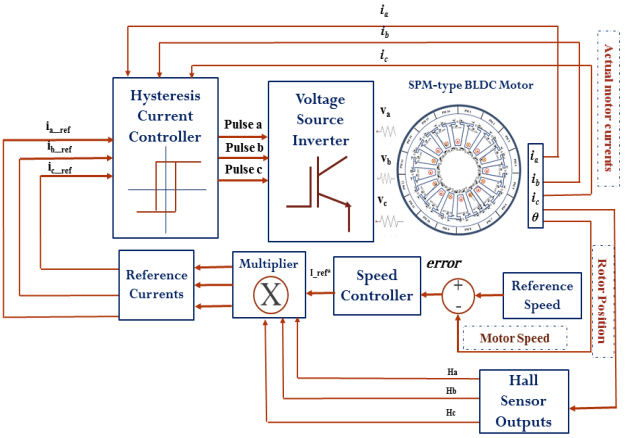

FIGURE 3. Equivalent BLDC motor drive operation under 120-degree and constant power conduction mode.

However, during Stator Inter-Turn Fault (SITF) conditions in a machine, the insulation breakdown undergoes the change in resistance from infinity to a finite value which leads to the heavy inrush of current in the windings resulting in damage. The proposed study emulates the SITF conditions through the short-circuit of the winding coils with a finite resistance, R_f. The fault resistance is taken as $R_f = 0.1\ \Omega$. The resistance and inductances are split into two sub coils as shown in Fig. 4, to short circuit the turns of a winding.

For instance, the phase A winding is shorted at $\%\delta =$ 25-50% and the corresponding inductance for healthy and faulty parts are referred as L_{a1} and L_{a2} respectively. The mutual inductance is represented as M_{a1a2} and given from (9)-(11).

$$L_{a1} = (1-\delta)^2 L_a \tag{9}$$

$$M_{a1a2} = \delta(1-\delta) L_a \tag{10}$$

$$L_{a2} = (\delta)^2 L_a \tag{11}$$

where δ represents the fraction per unit of faulty turns. The L_s under healthy conditions is given in Fig. 4.

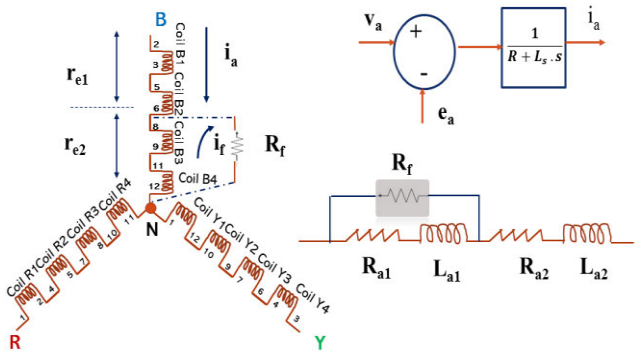

FIGURE 4. Modeling of SITF conditions in a stator winding of a BLDC motor having through splitting of two sub-coils.

The voltage dynamics in (1) therefore, transforms during the fault conditions and is given through (12).

$$[V_s] = [R_s]\,[I_s] + [L_{ss}]\,\frac{d[I_s]}{dt} + [E_s] - [R_0]\,i_f - [L_0]\frac{di_f}{dt} \tag{12}$$

Here, $[V_s]$, $[I_s]$ and $[E_s]$ are the stator voltage, current and back-EMF vectors. R_s is the phase resistance and $[L_{ss}]$ is the inductance matrix of the healthy BLDC motor respectively. $[R_0]$ and $[L_0]$ are the fault resistance and inductance matrix in the faulty part of the winding. The detailed expressions and equations can be referred from [12], [15], [16].

However, the fault current between the insulation fault resistance, r_f referred as i_f is given by (13):

$$R_{a2}i_a + (L_{a2} + M_{a1a2} - M_{a2b})\frac{di_a}{dt} + M_{a2b}\frac{di_b}{dt} + M_{a2c}\frac{di_c}{dt} + e_{a2} = (R_{a2} + r_f)i_f + L_{a2}\frac{di_f}{dt} \tag{13}$$

The L_s therefore changes during the SITF conditions which consequently drives the high rise in stator phase currents and alters the machine characteristic behavior. The adverse effect on the machine performance can be examined through the change in electromagnetic quantities encountered under healthy and subjected fault conditions given in Fig. 5. (a)-(c). The motor drive is operated at a speed of $\omega = 50$ rad/s and the corresponding back-EMF obtained is found to be $E_B = 4.5$V. The stator phase current and corresponding electromagnetic torque obtained is $I_S = 3.2$ A and $T_E = 0.6$ N-m. However, during the SITF conditions, the significant rise in average phase currents given in Fig. 5. (a), validates (13). The growth in magnitude of current corresponds to the fault current i_f across the shorted turns. The motor back-EMF tends to be out of phase undergoing a considerable change in frequency as shown in Fig. 5. (b). The back-EMF has a reduction of 1.125V in magnitude which is proportional to the percentage of shorted turns $\%\delta$. Since the mechanical speed is directly proportional to the motor back-EMF, therefore any change in motor back-EMF have a direct impact on the rotating speed. During SITF conditions the motor speed decreases and consequently its frequency changes causing unsteadiness and

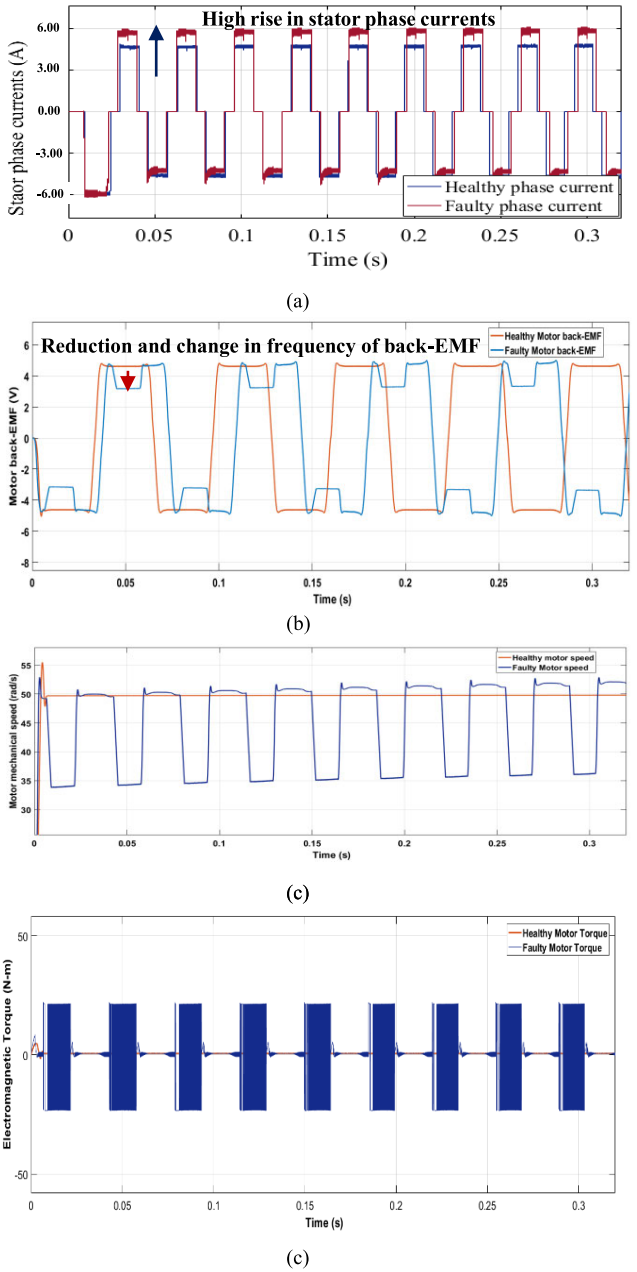

FIGURE 5. (a) Stator phase currents under healthy and SITF conditions. High rise in Is signify the short circuit of stator winding. (b) Reduction and change in phase sequence of rotor back-EMF. (c) Unsteadiness in mechanical speed under SITF conditions. (d) High ripples in motor electromagnetic torque for SITF conditions.

oscillations as given in Fig. 5. (c). In addition, the electromagnetic torque encounters high ripple content in its signature shown in Fig. 5. (d).

The IWFT and EEC based approach of modeling the SITF conditions in a BLDC motor, gives fairly good results to detect and diagnose the existence of fault in a machine. The method involves less computational time but compromises on accuracy. Therefore, the Numerical Method (NM) based approach is preferred to study more accurate outcomes of a machine under subjected fault conditions. However, the NMs takes more computational time for analysis.

B. NUMERICAL METHOD (NM) BASED MODELING APPROACH

A numerical model of a BLDC motor under SITF conditions is developed using the Finite Element (FE)-Simplorer based co-simulation approach. The Maxwell 2D/3D tool is used for developing a FE model of a BLDC motor while the Simplorer built the electric drive system for the motor operation. The complex modeling of the machine drive though involves a large computational time but yields more reliable solutions since the machine physical geometry, material properties and boundary conditions are taken into consideration during BLDC motor drive operations under subjected conditions. The outcomes thus obtained are explicit and possess high accuracy. The numerical model of a BLDC motor as shown in Fig. 6, is developed using the machine parameters given in Table. 1-2.

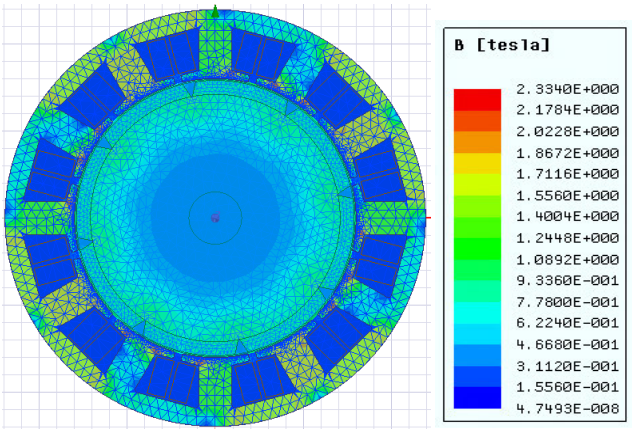

FIGURE 6. Meshed FE model of a BLDC motor showing healthy magnetic flux density (B_g) profile. The observed and accounted value is $B_g = 1.008$ T $\sim$ 1T.

TABLE 2. Numerical parameters of a BLDC motor.

Symbol	Quantity	Parameters
OD_S	Outer stator diameter	119.5 mm
ID_S	Inner stator diameter	80 mm
l_s	Length of stator	54 mm
PM	N35SH-Grade	NdFeB (SPM-type)
m_w	Width of magnet	4 mm
m_l	Length of magnet	50 mm
m_a	Magnet Angle	170 º
OD_R	Outer rotor diameter	78.95 mm
ID_R	Inner rotor diameter	15 mm
l_R	Length of rotor	50 mm
H_{s2}	Slot depth	13 mm
B_{so}	Slot opening	2.2mm
t_w	Tooth width	9.5 mm
t_a	Tooth tang angle	20 º

Similar to the operating conditions used in the preceding subsection-II-A, the FE-Simplorer based model is operated at a speed $\omega = 50$ rad/s. The healthy motor radial magnetic flux density (B_g) is found to be 1T as given in Fig. 7. (a) which is

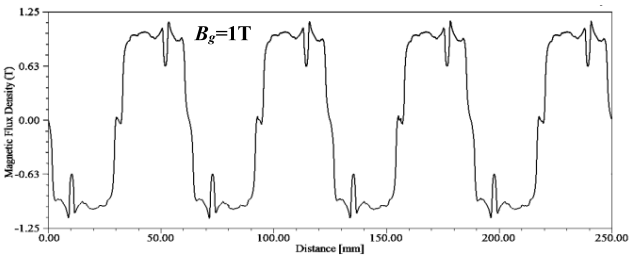

(a)

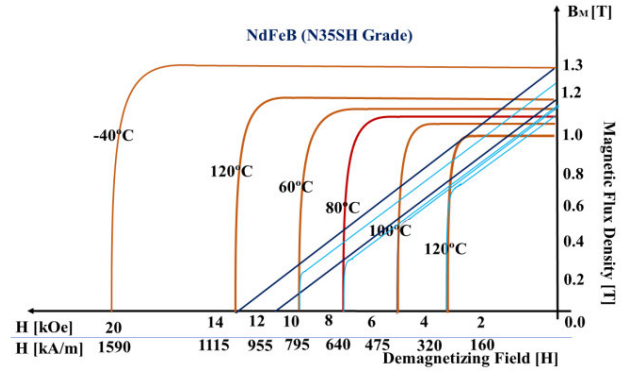

(b)

FIGURE 7. (a). Healthy radial magnetic flux density (B_g) profile for a BLDC motor, $B_g = 1$T. (b) BH curve of a PM (NdFeB of Grade N35SH) at different operating temperatures.

the according to the *BH characteristics* of N35SH grade PM for type NdFeB given in Fig. 7. (b).

The corresponding back-EMF is found to be $E_B = 4.5$V given in Fig. 8. (a). The stator phase current (*given as a square wave shaping*) and corresponding average electromagnetic torque obtained is $I_S = 3.2$ A and $T_E = 0.6$ N-m, given in Fig. 8. (b)-(c). However, during the SITF conditions which is emulated through the short-circuit of winding coils by a finite resistance, $R_f = 0.1\ \Omega$. The turns per coil $n_c = 6$. The coil_1 and coil_1re has been split into two sub coils shown in Fig. 9. Each disintegrated coil is assigned 2 turns while the parental coil is given 4 turns each (coil-1 and coil-1re) respectively. the rise in current corresponds to the shorted turns and is found to be more than 10A as shown in Fig. 10. (a). The similar rise current was earlier observed in hybrid model of a BLDC motor (Fig. 5.a). The E_B decreases significantly undergoing through the change in frequency as shown in Fig. 10. (b). The electromagnetic torque possesses high ripples shown in Fig. 10. (c) while the magnetic flux density (B_g) does not vary significantly under SITF conditions as given in Fig. 10. (d).

The numerical results are found to be in validation to the analytical outcomes obtained through IWFT and EEC based approach. However, the FE based results incorporates many assumptions of EEC based method such as material properties of the machine and therefore found to be more reliable and accurate. The subsequent section shall model the demagnetization effects in the BLDC motor using MEC and NM based approaches.

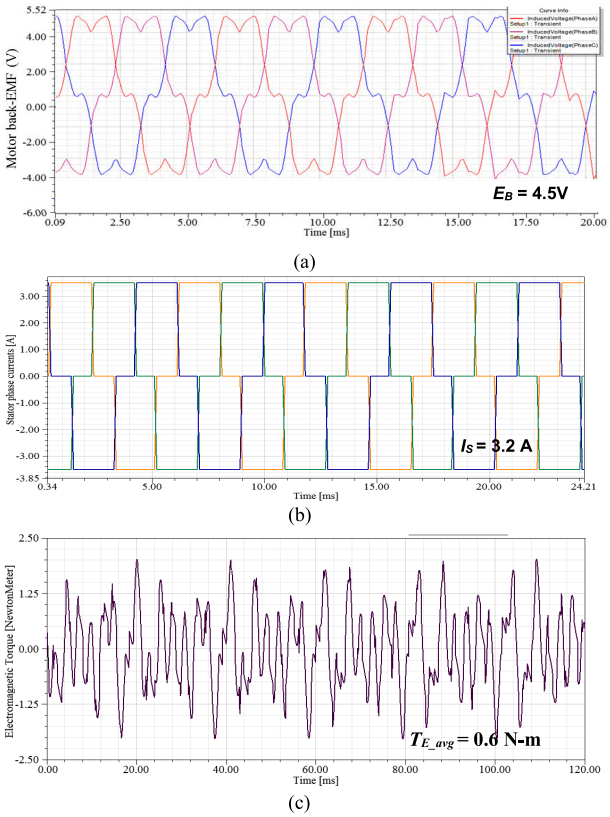

FIGURE 8. (a). Three Phase back-EMF of a motor with $E_B = 4.5$V [Phase A: Red, Phase B: Magenta, Phase C: Blue]. (b). Stator phase currents for a BLDC motor, $I_S = 3.2$ A. (c). Electromagnetic torque for a corresponding current, $T_E = 0.6$ N-m.

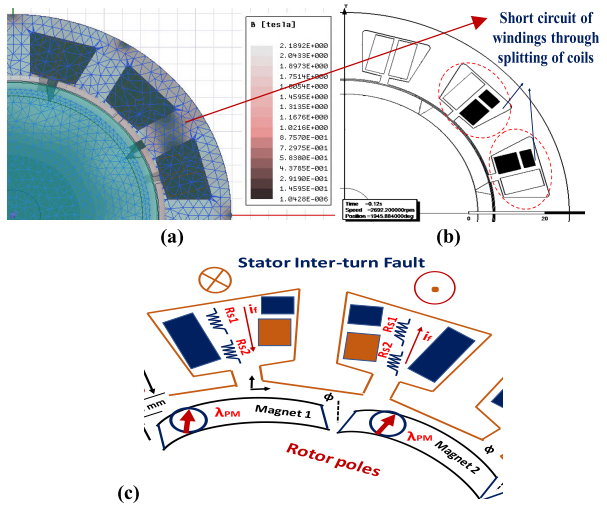

FIGURE 9. The meshed co-simulated model of a BLDC motor (quadrant view) showing two turns undergone SITF. (b) Splitting of a healthy coil into sub coil to emulate SITF conditions (c) MEC based model of SITF.

III. MODELING OF DEMAGNETIZATION EFFECTS IN ROTOR PMs OF A BLDC MOTOR

A. MAGNETIC EQUIVALENT CIRCUIT (MEC) AND NUMERICAL METHOD (NM) BASED ANALYSIS

As studied earlier in [1], [2], [17], [18] that for an unsaturated BLDC motor, the demagnetization curve is linear.

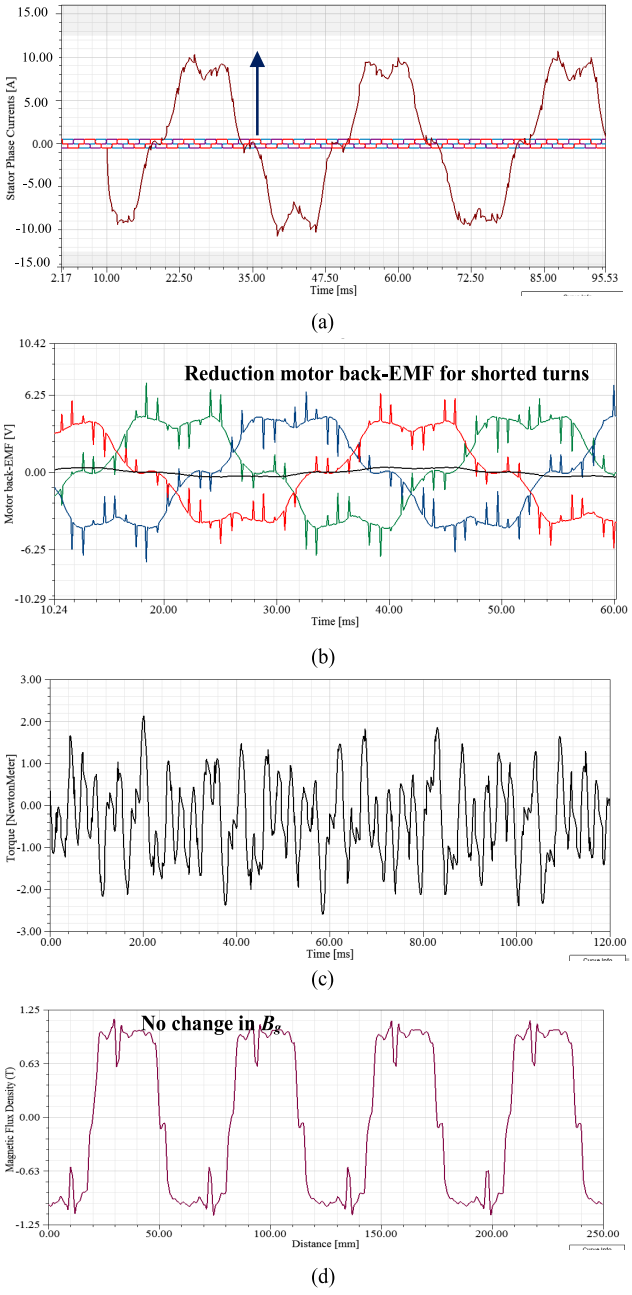

FIGURE 10. (a). Sudden high rise in phase current for the shorted windings. The current increases to more than 10A. (b). Reduction in back-EMF for the shorted turns during SITF conditions. (c). High rise accompanied with torque ripples during SITF conditions. (d). No significant change in magnetic flux density (B_g) during SITF conditions.

Therefore, the assumptions taken in the current study is that the permeability of the soft-magnetic material is infinite and the Neumann boundary condition where tangential magnetic field is zero) is applied at the boundary of the soft-magnetic material. The motor under study has PM of grade N35SH which has a linear second quadrant characteristic as shown earlier in Fig. 7. (b) is redrawn in Fig. 11. The equivalent MEC based circuit using LM and PN [18] approach has been developed as given in Fig. 12.

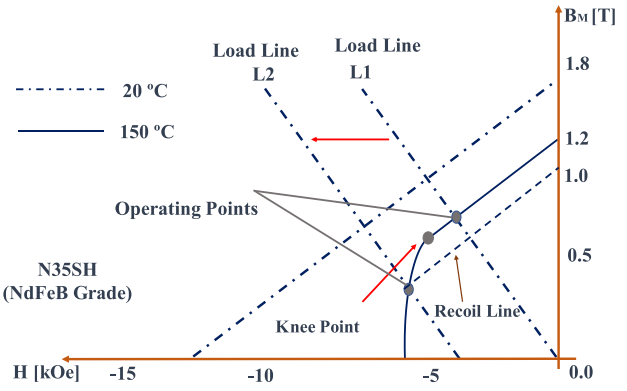

FIGURE 11. Linearized BH curve of a PM (*NdFeB of Grade N35SH*) at operating temperatures for demagnetization fault conditions.

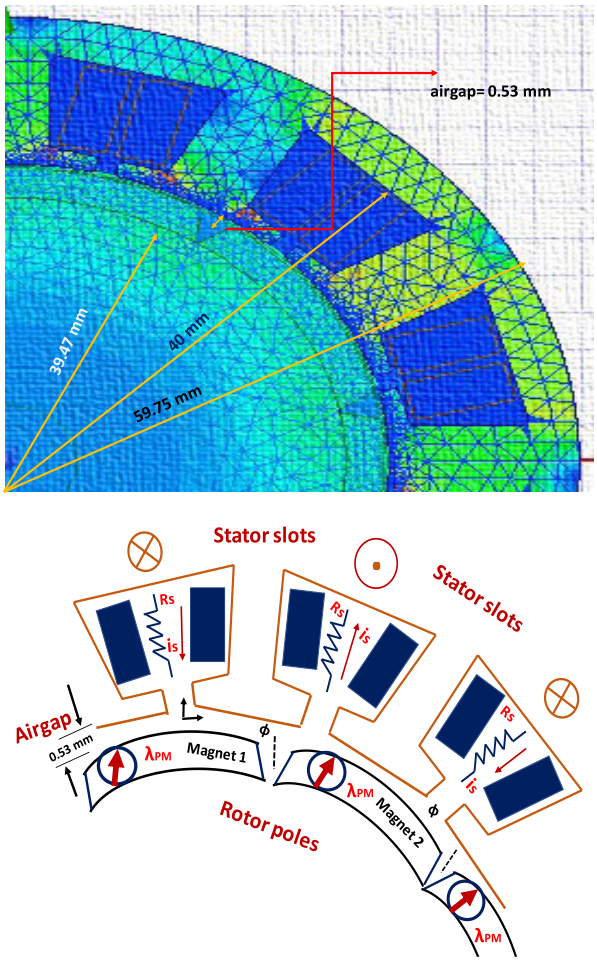

FIGURE 12. MEC based circuit using LM and PN approach for a SPM-type BLDC motor under study.

Calculation of Airgap Magnetic Fields ($\mathbf{B_g}$) *Based on MEC Calculus:* The radial component of the flux density can be given from (14) where B_g is an airgap flux density, B_r is residual flux density of PMs, g is an airgap length and h_m is the magnet thickness respectively.

$$B_g = \frac{B_r}{1 + \frac{g}{h_m}} \tag{14}$$

For a BLDC motor under study g is 0.53 mm, h_m is 4 mm and B_r is 1.2 T, which on substitution gives the desired value of $B_g = 1.05$ T. The radial magnetic flux density obtained earlier through FE analysis is found to be same as given in Fig. 7. (a).

B. NUMERICAL METHOD (NM) BASED MODELING APPROACH

The existence of high temperatures, unremitting mechanical stresses and aging of the rotor PMs gradually cause the magnets to lose its magnetic properties. A change in PMs magnetic coercivity (H_C) degrades its effectiveness which consequently inflict the demagnetization effect in the machine [1], [2], [13]. In the current study, the uniform demagnetization fault is emulated in the PM of a machine by changing its magnetic coercivity H_C uniformly for two adjacent poles (PMs). The flux density model of a BLDC motor under subjected demagnetization fault conditions is shown in Fig. 13, where two adjacent PMs undergoes change in magnetic coercivity H_C value. The healthy PM of grade N35SH possess the coercivity as, $H_C = 1082253$ A/m. Demagnetization effect is induced by changing the H_C through 40% and the new H_C reduces to 649352.16 A/m which is 60% of the healthy coercivity, as given in Table-3.

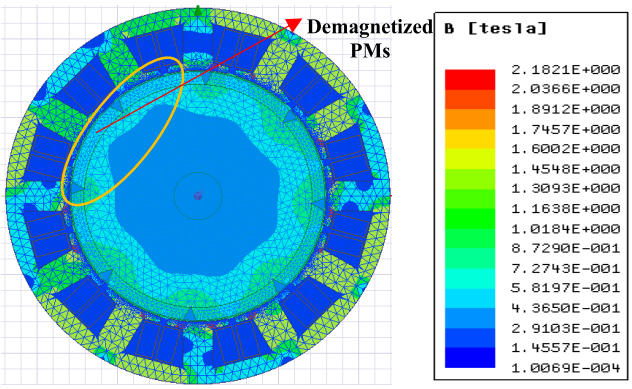

FIGURE 13. Meshed FE model of a BLDC motor showing uniformly demagnetized magnetic flux density (B_g) profile.

TABLE 3. Demagnetization parameters of a PM.

$H_{c\_healthy}$	1082253 A/m
H_{c_faulty}	649352.16 A/m (40% faulty and 60% healthy)

The proposed research, studies the rotor demagnetization effect by uniformly changing the PM's coercivity value under operating conditions. The change in machine quantities during the demagnetization fault is given from Fig. 14. (a)-(c). The significant and proportional changes in motor back-EMF and magnetic flux density can be seen from Fig. 14. (a)-(b)

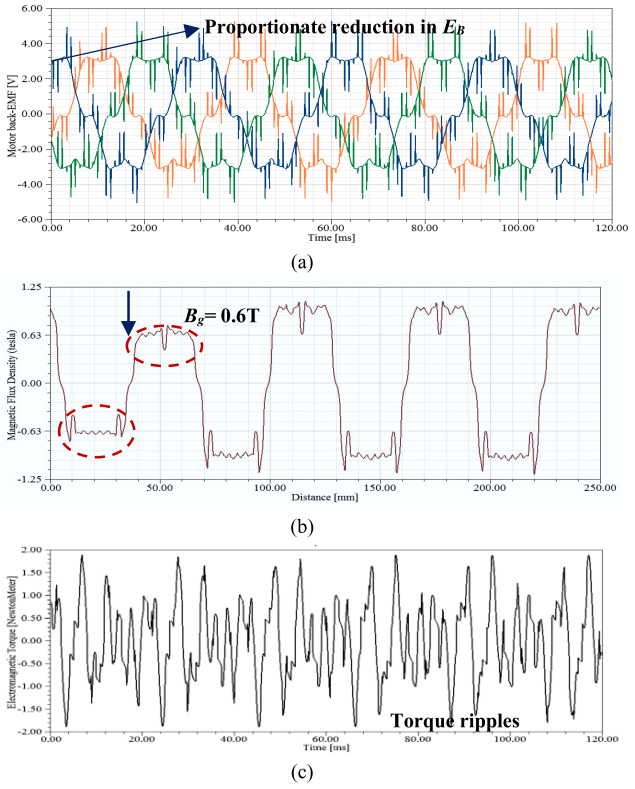

FIGURE 14. (a) Proportional change according to H_C in motor back-EMF during uniform demagnetization of PM in a machine. (b) Reduction in magnetic flux density value for the corresponding poles subjected to uniform emagnetization. The radal magnetic flux density is found to be $B_{g\_faulty} = 0.63$ T. (c) Variation in torque profile with an increase decrease pattern during demagnetization fault conditions.

respectively. The change and reduction in half cycles of B_g to approximately 40% for the corresponding poles which are subjected to uniform demagnetization, estimate the percentage loss in magnetism for the fault subjected PMs. The sharp peak ripples in the electromagnetic torque as shown in Fig. 14. (c), further signify the demagnetization effect in the machine.

The radial airgap magnetic flux density B_g and the winding inductances L_S obtained through MEC, NM and EEC based methods are now remodeled in the existing analytical model of a BLDC motor to develop a hybrid model system. The hybrid motor model possesses the analytically obtained winding inductance under SITF conditions and numerically achieved rotor magnetic fields subjected to rotor demagnetization fault effects as shall be discussed in the subsequent section.

IV. REMODELING OF L_S AND B_g TO DEVELOP A HYBRID MODEL SYSTEM FOR DIAGNOSIS OF FAULTS

The hybrid model system remodels the stator winding inductance L_S and rotor magnetic fields B_g in the EEC based develop BLDC motor model. The proposed system has significant advantages such as, it is efficient to model both the stator and rotor related machine faults in an existing analytically developed model which requires marginal transformation. Secondly the computational time required for analysis is considerably less when compared to high performance computation of FEA. In addition, the proposed system can model and analyze the combined effect of faults in a machine existing at the same time. The hybrid model system as shown in Fig. 15, shall therefore model the combined effect of both the faults in the machine through modeling of L_S obtained from IWFT based method and numerically modeled B_g under subjected fault conditions.

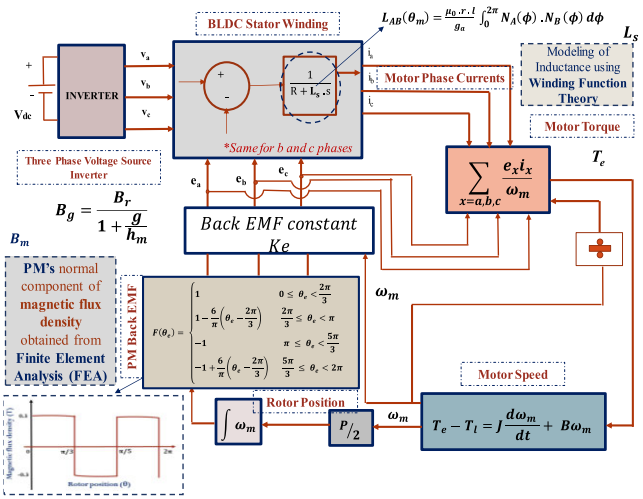

FIGURE 15. Hybrid BLDC motor model developed using the concept of remodeling of stator winding inductance (IWFT) and rotor magnetic fields (MEC and NM based method).

The distinguished outcomes thus obtained are used for the diagnosis and classification of faults in a BLDC motor drive under operating conditions. The hybrid model results are once again validated with the FE-Simplorer based co-simulation approach in order to authenticate the feasibility of the system. The subsequent subsection shall model the combined effect of SITF and rotor demagnetization faults in a hybrid BLDC motor drive and numerically through FE based analysis.

A. REMODELING OF L_S AND B_g IN THE DEVELOPED HYBRID SYSTEM

For the STIF conditions as modeled in Section. II-A, the stator winding inductance as calculated in (8)-(11) reduces and changes to $L_{sf} = 0.056$ mH as shown in Fig. 16.

Similarly, for the uniform demagnetization effects, the radial airgap flux density plot is extracted from the numerical simulation of a BLDC motor under open stator windings.

$$\lambda_{PM,a} = \int v_s dt \tag{15}$$

$\lambda_{PM,a}$ is the flux linkage of a PM for phase A given in terms of rotor back-EMF in (2) and (3). Referring the assumptions of section III-A, the B_g or E_B under demagnetization fault effects are deduced from (16)-(18), and the second quadrant

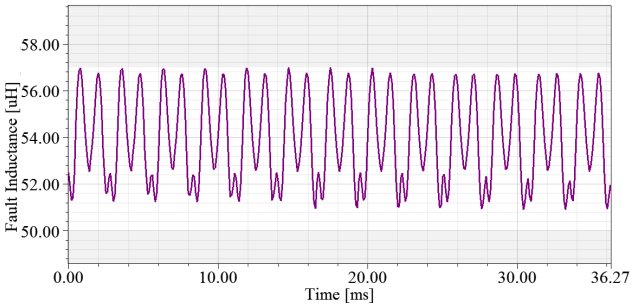

FIGURE 16. Stator winding inductance during SITF conditions.

BH characteristics curve of Fig. 11.

$$H_c l_m = \left(R_{MO} + R_g\right) * \phi_M \tag{16}$$

$$B_g = \frac{H_c l_m}{A * (R_{M0} + R_g)} \tag{17}$$

where $H_c l_m$ is a magnet's mmf, which is equal to the product of magnetic flux intensity (H_c) and mean flux path l_m, ϕ_M is the magnetic flux against the reluctance offered by the magnet given as R_{M0} and airgap, reluctance is denoted as R_g. Consequently, the rotor back-EMF, for phase-A is given as:

$$e_a = \frac{d\varphi_a}{d_t} = \frac{d\theta_r}{d_t}\frac{d\varphi_a}{d\theta_r} = \omega_m \frac{d\varphi_a}{d\theta_r} \tag{18}$$

where e_a is the back-EMF of phase A or the voltage induced in the stator coil, φ_a is a stator flux linkage in phase-A winding, θ_r is the angular displacement or rotor position and ω_m is the mechanical speed respectively. The radial airgap flux density, B_g plot obtained under uniform demagnetization of two adjacent poles is given in Fig. 17.

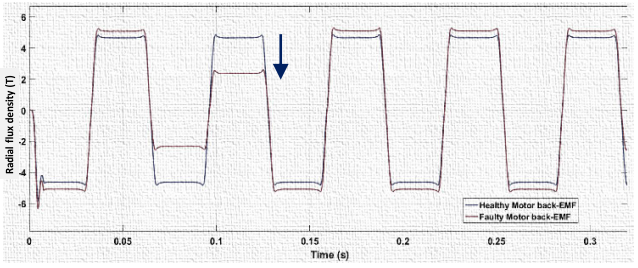

FIGURE 17. Magnetic flux density profile under uniformly demagnetized rotor PMs of a BLDC Motor.

The SITF conditions (L_s) and the rotor demagnetization effects (B_g) are remodeled in the hybrid system shown through Fig. 15 & 18, as a combined fault effect. The performance characteristics of a machine under subjected fault conditions are given in Fig. 19. (a)-(c).

The machine quantities undergo *doubly effect change* during the combined effect of faults. For instance, the high rise in stator phase current possessing an oscillatory behavior (with increase-decrease pattern) in I_S signature shown in Fig. 19. (a), signify the SITF conditions coupled with demagnetization effect. The reduction in motor back-EMF

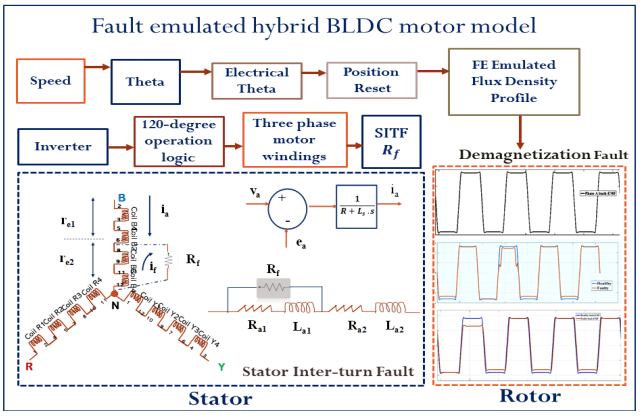

FIGURE 18. Combined effect of SITF and demagnetization fault conditions modeled in a hybrid motor model system.

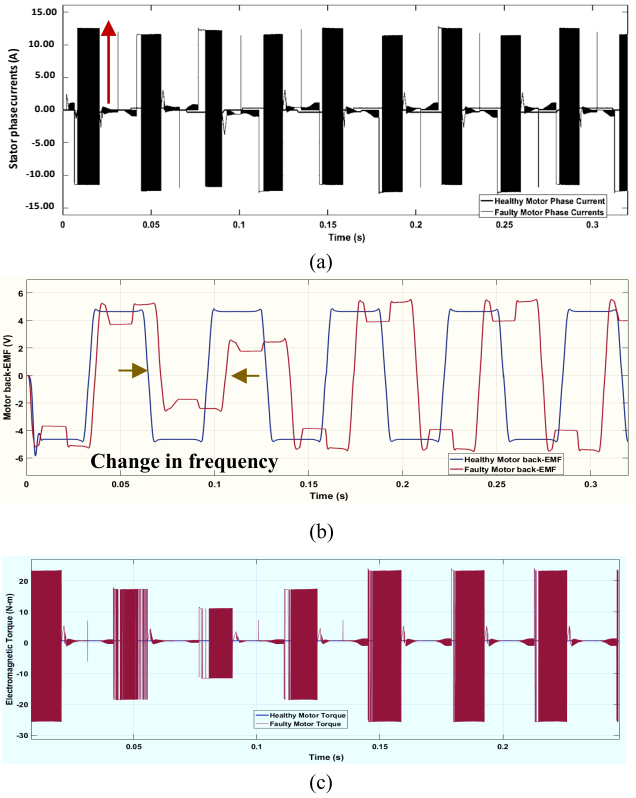

FIGURE 19. (a) High rise in phase currents increases for the combined SITF and uniform demagnetization faults in the BLDC motor. (b) Equivalent reduction in E_B for a corresponding half-cycles (poles) signifies the subjected demagnetized PMs. The change in frequency validates the combined effect of SITF with the demagnetization faults in the BLDC motor. (c) Combined effect of fault has double affect in motor torque for a BLDC motor.

has a combined effect of both the faults where the decrease in magnitude for two corresponding poles signify demagnetization fault while the average marginal reduction in every half cycle validates the SITF effect in the windings as shown in Fig. 19. (b). In addition, the combined fault effect has a change in frequency for motor back-EMF signifying the effect of SITF conditions in the existing demagnetized state of

a machine. Further, the electromagnetic torque of the machine possesses oscillations and change in frequency with high ripples showing the effect of both the faults in the machine as shown in Fig. 19. (c).

The adverse effect in the machine quantities are distinct and distinguishes from individual fault effects which further aid in identifying and giving a classification to motor faults. The outcomes obtained are further validated with the numerical modeling approach where the FE model of both the SITF and demagnetized motor is subjected to operating conditions to observe the *doubly effect changes* in machine quantities.

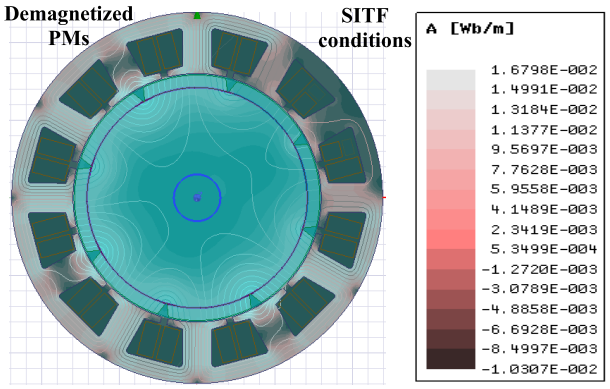

FIGURE 20. Combined effect of SITF and demagnetization fault conditions in a numerically developed BLDC motor. (Flux model).

B. COMBINED MODELING OF L_S AND B_g IN THE NUMERICALLY DEVELOPED BLDC MOTOR

The combined effect of SITF and demagnetization faults (*numerically modeled earlier as individual faults in Section II-B and III-B*) are now emulated together in the FE developed BLDC motor as show in Fig. 20.

During the combined fault effect, the high rise in current is more than 10A since the corresponding current across the shorted turns has an additional increase in current compensating the fall in rotor back-EMF due to demagnetization of PM (constant power operation). The rise in current is accompanied with a change in frequency as shown in Fig. 21. (a). This signifies the coexistence of SITF and demagnetization fault effect in the machine, studied and analyzed in the preceding section. In addition, the proportionate reduction in back-EMF is found to be same as the percentage loss of H_c (40% reduction in E_B) in the PMs while the back-EMF across the shorted windings is significantly less (1.125 V), undergoing through the change in frequency as shown in Fig. 21. (b), signifying SITF conditions and validating the proposed postulations. The reduction and distinguishing pattern in electromagnetic torque as shown in Fig. 21. (c), signifies the combined fault effect. In addition, the expected change in radial magnetic flux density $\boldsymbol{B_g}$ as encountered in Fig. 21. (d), itself validates that there is a demagnetization effect in the machine since the change in $\boldsymbol{B_g}$ is not observed during the individual SITF conditions existing in a machine.

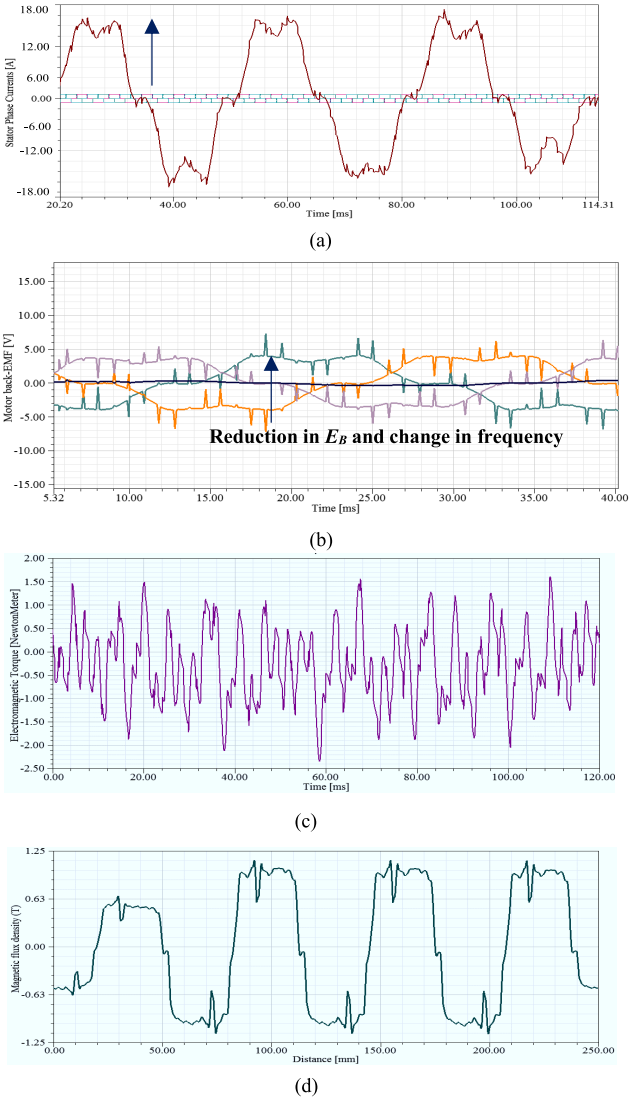

FIGURE 21. (a) High rise in current corresponding to shorted turns accompanied with change in frequency during the combined effect of SITF and demagnetization fault in a machine. (b) Reduction and change in frequency of back-EMF during combined effect of SITF and uniform demagnetization conditions. (c) Oscillatory behavior with and increase and decrease in magnitude of torque during SITF and demagnetization fault conditions. (d) Reduction in magnetic flux density value during combined effect of SITF and uniform demagnetization fault.

Thus, since change in $\boldsymbol{B_g}$ characterizes demagnetization fault in the machine, the change in frequency of E_B validates the SITF conditions, signifying the combined effect of fault in the machine. It has been investigated that, among other adverse effect in electromagnetic signatures, the significant and distinct changes encountered in *rotor back-EMF* and *radial magnetic flux density* gives more simple identification and classification to motor faults.

In addition, before proceeding to the experimental investigations, the subsequent section illustrates briefly the harmonic analysis of phase currents and back-EMF of a BLDC motor under healthy and demagnetization fault conditions. The harmonic based analysis though is beyond the scope

of the current study; however, it is included to develop a framework for the future research investigations.

V. HARMONIC ANALYSIS OF A BLDC MOTOR UNDER HEALTHY AND FAULT CONDITIONS

Additional investigations are made on the harmonic analysis of demagnetization faults in the BLDC motor drive. The harmonics are excited at multiples of mechanical frequency in the stator back-EMF and current spectrum as given in (19).

$$f_f = \left(\frac{k}{P/2}\right) f_s = k f_m \quad k = 1, 2, 3 \ldots . \tag{19}$$

where f_f is the frequency of k^{th} component in the spectrum, f_s is electrical frequency, f_m is the rotational frequency and p is the number of poles. The proposed investigations are done on the BLDC motor under study with $p = 8$ which is operated at mechanical speed of $\omega_m = 50$ rad/s (as for all operating conditions). The corresponding electrical and mechanical frequency thus calculated is found to be, $f_s = 32$ Hz and $f_m = 8$ respectively. The harmonic analysis is performed by taking the fundamental frequency as electrical frequency i.e. 32 Hz and is being shown through Fig. 22-23. The presence of harmonics with the multiple of mechanical frequency (f_m) are also encountered and presented.

A. HARMONIC ANALYSIS UNDER HEALTHY CONDITIONS

The harmonic analysis of stator phase currents and rotor back-EMF are analyzed at fundamental electrical frequency ($f_s = 32$ Hz) as shown in Fig. 22. (a)-(b). The motor current THD is found to be 30.16% (Fig. 22. (a)) while the harmonic characteristics of the motor back-EMF is 36.21% THD (Fig. 22. (b)).

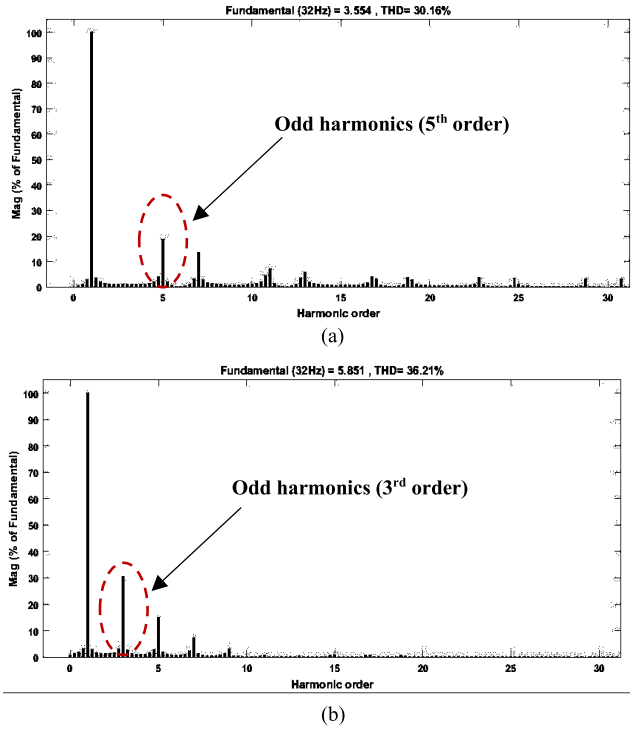

FIGURE 22. (a) Harmonics in the current relative to fundamental at $f_s = 32$ Hz for healthy BLDC motor. (b) Harmonics in the back-EMF relative to fundamental at $f_s = 32$ Hz for healthy BLDC motor.

B. HARMONIC ANALYSIS UNDER FAULT CONDITIONS

The harmonic analysis of stator phase currents and rotor back-EMF under fault conditions *(here uniform demagnetization conditions are taken for analysis)* has been already illustrated in Fig. 23. (a)-(b). the motor current THD is found to be 35.93% (Fig. 23. (a)) while the harmonic characteristics of the motor back-EMF is 39.28% THD (Fig. 23. (b)).

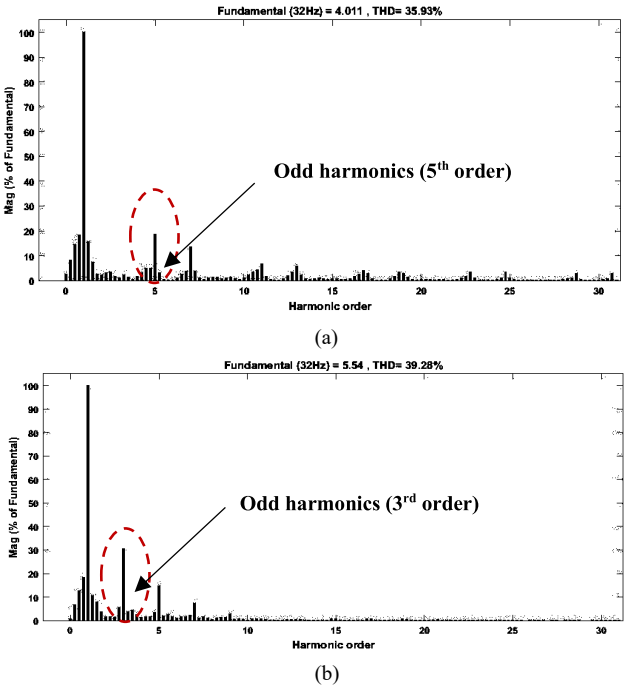

FIGURE 23. (a) Harmonics in the current relative to fundamental at $f_s = 32$ Hz during uniform demagnetization of BLDC motor. (b) Harmonics in the back-EMF relative to fundamental at $f_s = 32$ Hz during uniform demagnetization of BLDC motor.

The harmonic components of motor back-EMF and stator phase current is summarized in Table 4-5. It can be observed that the $3^{rd}(k = 12)$, $5^{th}(k = 20)$ and $7^{th}(k = 28)$ harmonics of back-EMF of fundamental electrical frequency ($f_s = 32$ Hz) are almost same for both the healthy and fault conditions but the difference can be observed in other harmonic components. It has been also observed that the back-EMF has dominant 3^{rd} harmonic component while it is negligible in motor current. This is one of the significant distinct characteristics to classify the fault in a BLDC motor.

VI. EXPERIMENTAL VALIDATION TO THE PROPOSED FAULT MODELING APPRAOCHES AND CLASSIFYING THE MACHINE FAULTS

The experimental investigations are carried out on a closed loop BLDC motor drive developed using a FPGA

TABLE 4. Harmonic components of back-EMF signatures.

Harmonic Frequency (k f_m)	8 Hz (k =1)	16 Hz (k =2)	24 Hz (k =3)	32 Hz (f_s)	40Hz (k =5)	48 Hz (k =6)	96 Hz (k =12)	160 Hz (k =20)	224 Hz (k =28)
Healthy conditions	1.40%	1.83 %	3.13 %	100 %	2.89 %	1.69 %	30.68 %	15.14 %	7.52 %
Fault conditions	6.7 %	12.82 %	18.36 %	100 %	10.52 %	7.81 %	30.51 %	14.89 %	7.30 %

TABLE 5. Harmonic components of stator current signatures.

Harmonic Frequency (k f_m)	0 Hz (k =0)	8 Hz (k =1)	16 Hz (k =2)	24 Hz (k =3)	32 Hz (f_s)	40Hz (k =5)	48 Hz (k =6)	160 Hz (k =20)	224 Hz (k =28)
Healthy conditions	0.02 %	0.41 %	1.03 %	2.71 %	100 %	3.46 %	1.98 %	18.67 %	13.47 %
Fault conditions	2.61 %	8.15 %	14.48 %	18.3 %	100 %	15.75 %	7.23 %	18.52 %	13.48 %

(Spartan 6) based real–time control system. The control system is designed using a hysteresis current control (HCC) technique for deriving the switching pulses for 120-degree conduction Voltage Source Inverter (VSI). The controller is programmed using Hardware Description Language (HDL) for interfacing with the three phase windings of a BLDC motor. The inner rotor SPM-type BLDC motor with HE/flux sensors embedded on stator periphery as shown in Fig. 24. (a)-(b) undergoes change in PM properties in order to induce demagnetization effects in the machine.

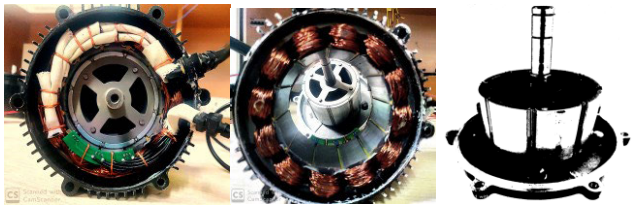

(a) (b) (c)

FIGURE 24. (a) Three phase BLDC motor showing outer-stator, inner-rotor and the hall-effect/magnetic flux sensors. (b) Stator with 12 slots having three-phase star connected windings (c) 8-pole rotor having surface mounted PM (SPM).

a. The two adjacent PMs of Motor-1 has been uniformly demagnetized to a demagnetization factor of approximately $\psi = 40\%$ (similar to modeling approach). The demagnetization has been carried out during the development of a motor drive, in a heating chamber at the temperatures above 150° C. The demagnetization of N35SH PM follows the corresponding demagnetization *BH characteristic* as given earlier in Fig. 7. (b) and Fig. 11. Similar BH curve is obtained numerically, when plotted using FE method as shown in Fig. 25. The embedded flux sensors are programmed through HDL and HE sensors to measure the airgap B_M and record the data through Data Acquisition (DAQ) system.

The demagnetized rotor is then assembled in the stator maintaining an airgap of 1mm. **b.** The Motor-2 has tapings

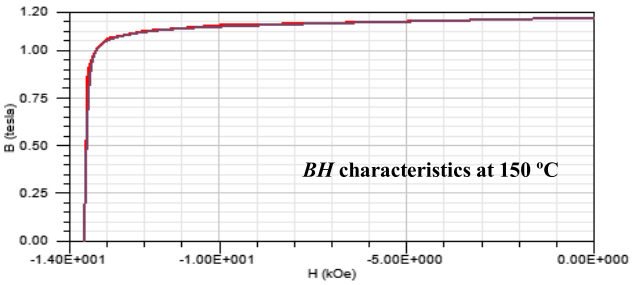

FIGURE 25. BH characteristics of a PM at 150° C (PM of grade-N35SH) obtained through FE analysis.

in the stator windings at 25% intervals of complete winding in each phase shown in Fig. 26 and Table-6. This motor is used for healthy operations (when tapings are not shorted) and SITF conditions. **c.** The Motor-3 has demagnetized rotor (of Motor-1) and a stator with tapings (of Motor-2) to investigate the combined effect of both the faults. The complete experimental testbed with healthy and faulty BLDC motor operations has been set up as given in Fig. 27.

The testbed comprises of three phase Voltage Source Inverter (VSI), FPGA based controller, healthy and fault emulated BLDC motors and DAQ system for recording the motor characteristic signatures.

A. BLDC MOTOR PERFORMANCE UNDER HEALTHY CONDITIONS

The motor-drive is operated at $\omega_m = 50$ rad/s and the current and back-EMF for a healthy BLDC is observed to be 3.5 A and 4.5V respectively as shown in Fig. 28. (a). The assertion of motor back-EMF (E_B) as magnetic flux density (B_g) and is found to be 1T ($B_g = K_E{}^*\omega_m$) as shown in Fig. 28. (b). Here $K_E = 0.02$ V/rad/s (or T/rad/s). Similar results were obtained through proposed modeling and simulation-based analysis.

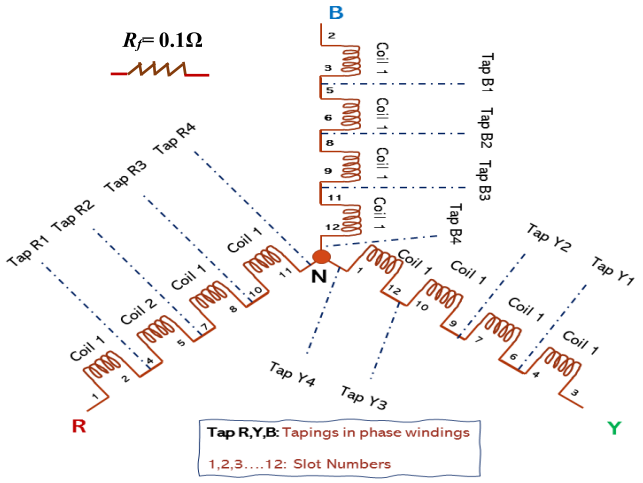

FIGURE 26. Three phase stator windings of a BLDC motor showing winding arrangement and tapings percentage to emulate SITF effects.

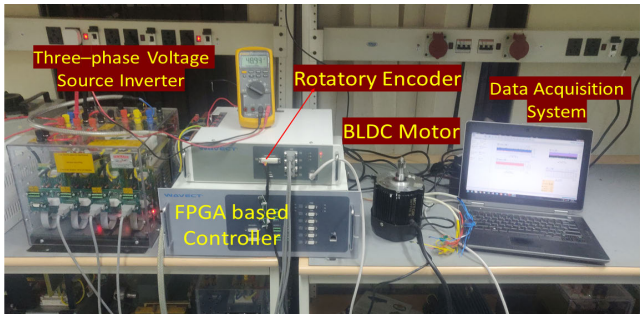

FIGURE 27. Complete experimental setup with i. healthy ii. SITF iii. demagnetized iv. combined SITF and demagnetization fault emulated BLDC motor.

TABLE 6. Percentage tapings in stator windings of a BLDC motor.

Short-circuit Percentage	R Phase	Y Phase	B Phase
25%	Tap R1	Tap Y1	Tap B1
50%	Tap R2	Tap Y2	Tap B2
75%	Tap R3	Tap Y3	Tap B3
100%	Tap R4	Tap Y4	Tap B4

B. BLDC MOTOR PERFORMANCE UNDER SITF CONDITIONS

For the BLDC motor operation under SITF conditions, the expected sudden rise in stator phase currents is observed as shown in Fig. 29. (a). The corresponding change in motor back-EMF is given in Fig. 29. (b). The similar outcomes have been encountered in Section-II using the EEC-IWFT based modeling approaches.

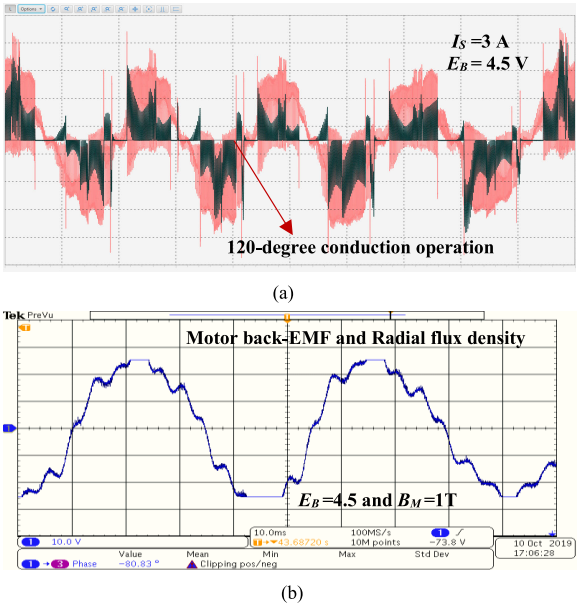

FIGURE 28. (a) *Experimentally* obained healthy motor back-EMF $E_B = 4.5$ V and phase c urrents $I_{ph} = 3$ A [$V_{ac} \sim 2V/div$ (*pink*), $I_{ph} \sim 5A/div$ (*green*), $t = 20\ ms/div$]. (b) *Experimentally* obained healthy motor back-EMF $E_B = 4.5$ V [$V_{ac} \sim 2V/div$(*blue*), $t = 20ms/div$]. The same has been plotted to obtain radial flux density using flux sensors, accounting for $B_g = 1$T [0.5T/div].

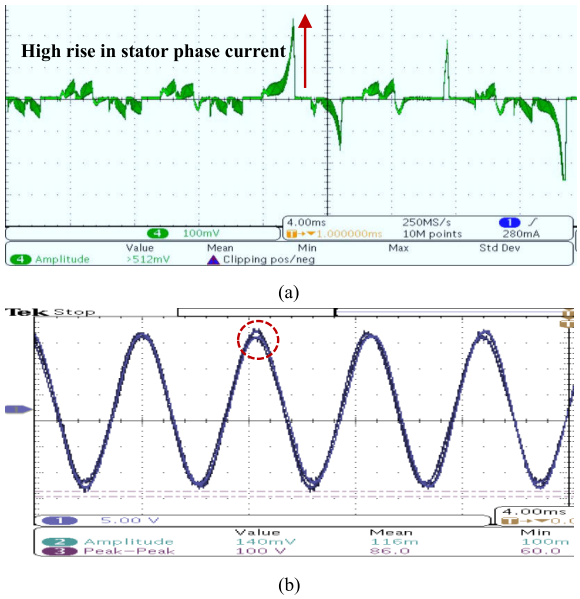

FIGURE 29. (a) *Expremently* obtained high rise in stator phase current (phase-A) under SITF condition [$V_{ac} \sim 2V/div$, $I_{ph} \sim 5A/div$, $t = 10ms/div$]. (b) *Expremently* obtained rotor back-EMF under SITF conditions [$V_{ac} \sim 2V/div$, $t = 10ms/div$]. The sinusoidal shape of back-EMF is due to the curved shape of the PMs of Motor-2.

C. BLDC MOTOR PERFORMANCE UNDER DEMAGNETIZATION FAULT CONDITIONS

For a demagnetized fault emulated BLDC motor operation, the rise in phase currents and the proportionate change in back-EMF (E_B) or radial magnetic flux density (B_g) are

observed as shown in Fig. 30. (a)-(b). It is found that the B_g decreases in the same proportion as the induced change in magnetic coercivity (H_C) value. The back-EMF (E_B) for the demagnetized pole, reduces by 40% and is found to be 2.7 V (healthy $E_B = 4.5$ V) which is approximately 40% of healthy back-EMF. The same has also been validated earlier in Section III of this paper.

(a)

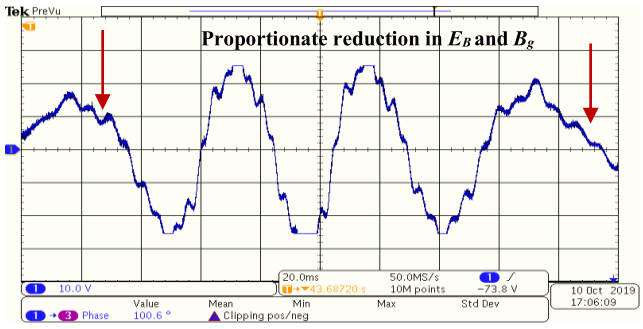

(b)

FIGURE 30. (a) *Experimentally* obained uniformly demagneized PMs' back-EMF (E_B) and phase current [$V_{ac} \sim 2V/div(red), I_{ph} \sim 1A/div(green), t = 10ms/div$] (120-degree conduction). (b) *Experimentally* obrained back-EMF (B_g) for corresponding uniformly demagnetized PM, found to be $E_B = 2.7$ V [$V_{ac} \sim 2V/div, I_{ph} \sim 2A/div, t = 10ms/div$]. The same has been plotted to obtain radial flux density under demagnetization fault conditions, accounting for approximately $B_{g\_faulty} = 0.6T$[$0.5T/div$].

D. BLDC MOTOR PERFORMANCE UNDER COMBINED EFFECT OF SITF AND DEMAGNETIZATION FAULT CONDITIONS

For the BLDC motor operation under combine effect of SITF and demagnetization fault conditions, the stator phase current possess the oscillatory rising behavior with an increase-decrease pattern as shown in Fig. 31. (a). The motor back-EMF across the shorted windings is significantly less, undergoing through the change in frequency as shown in Fig. 31. (b), thereby signifying SITF and demagnetization fault conditions in the machine.

The experimental outcomes thus obtained are similar when compared with the results obtained earlier using the proposed hybrid model-based approach.

VII. DEDUCTIONS AND CLASSIFICATION OF FAULTS

The proposed research carries out an extensive investigation on the Stator Inter-Turn Faults (SITFs), demagnetization

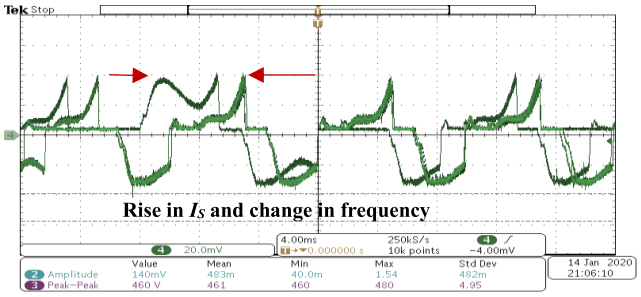

(a)

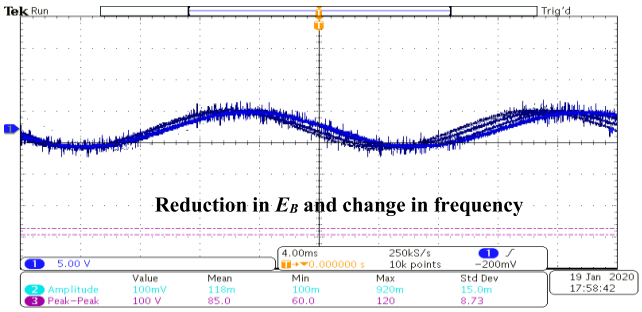

(b)

FIGURE 31. (a) *Experimentally* obtained oscillating high rise in phase current for combined SITF and demagnetization fault conditions in BLDC motor operation [$V_{ac} \sim 2V/div, I_{ph} \sim 5A/div, t = 4ms/div$]. (b) *Experimentally* obained back-EMF (B_g) for combined SITF and demagnetization fault conditions in BLDC motor operation [$V_{ac} \sim 2V/div, I_{ph} \sim 5A/div, t = 10ms/div$].

effect and combined effect of both the faults on the BLDC motor drive. The fault analysis is done using the proposed EEC (IWFT), MEC (LM and PN), NM (FE) and hybrid model based approaches respectively. The simulation outcomes are further validated experimentally. The results thus obtained reveals that during the existence of faults, the performance of the machine degrades due to the adverse effect in the electromagnetic quantities of the motor. The significant changes observed in the stator phase currents (I_s), motor back-EMF (E_B) and electromagnetic torque (T_E) suspects the existence of fault in the machine. The additional changes encountered in the magnetic quantities of the machine, such as radial magnetic flux density (B_g) further confirms the type and gives classification to the fault.

A. MOTOR CURRENT SIGNATURE (I_S)

During the SITF conditions, the stator current, I_S suddenly rises in a very short interval of time. The rise in current corresponds to shorted turns as can been seen from Fig. 5. (a) (EEC) and Fig. 10. (a) (NM). The breakdown of winding insulation is validated with the instant rise in stator phase currents, signifying the SITF conditions. But for a demagnetization fault, the rise in current is not significant. However, when both the faults viz. SITF and demagnetization occurs together, the rise in current possess change in frequency, thereby signifying the combined effect of the faults as also shown in Fig. 19. (a) and Fig. 21. (a)

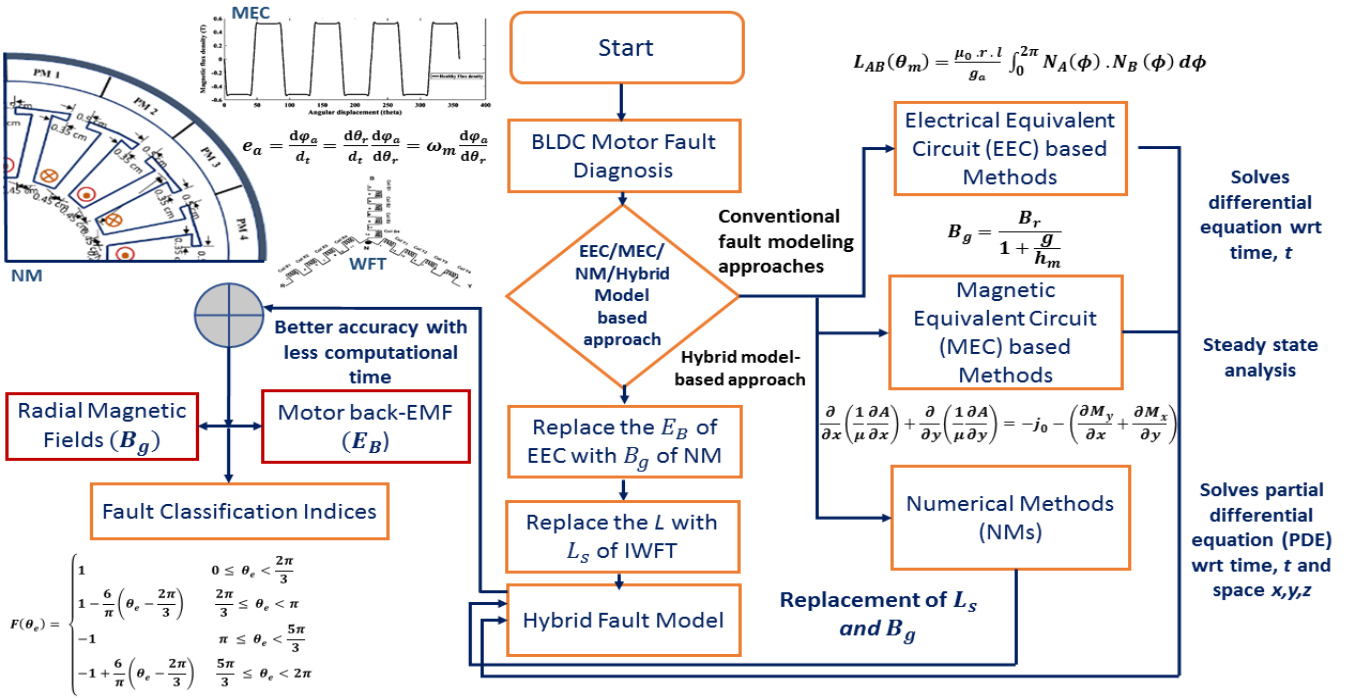

FIGURE 32. Flowchart for effective diagnosis and classification of machine faults using conventional and hybrid fault modeling approaches. The inference is made depending on the accuracy and computational time-based analysis.

B. MOTOR BACK-EMF SIGNATURE (E_B)

The motor back-EMF during SITF conditions reduces in proportion to the percentage of short circuit turns. In the proposed study the short circuit is emulated for $\delta = 25\%$ and the winding turns undergoes the decrease in E_B proportionally. For the demagnetization fault where approximately 40% magnetic coercivity has been reduced in the PMs of the machine, the corresponding half-cycles of the back-EMF reduces (to 2.7V) proportionally as shown in Fig. 5. (b) and Fig. 21. (b). This validates the assertion taken in the proposed study and also in (16)-(18) of the healthy and faulty back-EMF relation. The correlation is further deduced through (20):

$$e_{b\_faulty} = \psi(e_{b\_healthy}) \tag{20}$$

where ψ is the demagnetization factor.

Moreover, during the combined fault effect, the average reduction in back-EMF encounters the adverse effect of both the SITF and demagnetization fault respectively.

C. RADIAL MAGNETIC FLUX DENSITY (B_g)

It has been observed that during the SITF, the change in B_g is not much significant however during the demagnetization fault, the B_g is in proportion to the change in magnetic coercivity as shown in Fig. 10. (d) and Fig. 14. (d). However, under the combined fault effect, the change in B_g is not proportional as given in Fig. 21. (d), which signifies the occurrence of a demagnetization fault accompanied with the SITF effect.

Therefore, the detrimental changes encountered for the corresponding faults in terms of stator phase currents (I_s), motor back-EMF (E_B) and radial magnetic flux density (B_g), further confirms the type and gives classification to the machine faults. In addition, the subsequent section discusses the accuracy and computational time-based performance of the proposed modeling techniques for the diagnosis of faults.

VIII. ACCURACY AND COMPUTATIONAL TIME-BASED ANALYSIS

The outcomes secured through the EEC, MEC, NM and hybrid model-based approaches validate the experimental investigations carried out in support to the proposed fault modeling methods. It was found that the numerical results are almost similar to the experimental outcomes than the EEC and MEC based results. However, the results accomplished through the proposed hybrid model approach, are fairly proficient in diagnosing and classifying the faults. In addition, the results accomplished have better accuracy than the conventionally used EEC and MEC based methods and are faster than the NM based approaches, thereby effectively detecting the fault in its incipient stage. However, the choice of fault modeling methods can be chosen based on accuracy-computational time-based analysis as given in Fig. 32.

Modeling of BLDC motor faults using IWFT and EEC based approaches requires less computational time since the analytical methods considers several assumptions like neglecting the material properties and eddy current effects. The electrical quantities of the machine are calculated on

TABLE 7. BLDC motor faults diagnosis & classification.

Type of BLDC Motor Fault	Phase Currents (A) *[I_S]*	Back-EMF (V) *[E_B]*	Electromagnetic Torque (N-m) *[T_E]*	Magnetic Flux Density (T) *[B_g]*
Stator Inter-Turn Fault (SITF)	Sudden high rise in stator phase currents	Significant decrease in back-EMF for the corresponding shorted turns	Varying high torque ripples	No significant change
Uniform Demagnetization Fault	Insignificant rise in current	Reduction in back-EMF in proportion to the change in magnetic coercivity (presence of 3rd harmonics)	Torque ripples of varying frequency domain	Reduction in magnetic flux density in accordance with the change in demagnetizing factor (magnetic coercivity)
Combined Effect of Faults	The oscillatory and significant rise in current is observed with the change in frequency spectrum	Change in back-EMF frequency signifying SITF while the proportionate reduction in back-EMF with respect to the change in H_C signifies demagnetization fault	The torque has a fluctuating increasing pattern showing distinguishing behavior	The change in B_g is not proportional to the change in H_c which signifies the occurrence of a demagnetization fault accompanied by SITF

the basis of machine geometry. As studied in section- II, for modeling the SITF conditions, the machine parameters like winding inductances are calculated using the winding layout of the motor which requires the physical geometry of the machine. The results accomplished involves less computational time since the differential equations are solved with respect to time only, and therefore the speed of computational is significantly fast.

In contrary, the MEC based methods gives fairly good results with optimum computational time involved in analysis. As studied in section-III, the motor is converted into an equivalent magnetic circuit to find machine flux related quantities (which involve machine's physical geometry and material properties) such as magnetic flux linkages and flux density. The results thus accomplished subdues several limitations of the EEC based methods and therefore gives results with comparatively better accuracy and taking more computational time.

However, when the faults are modeled using the NM based approaches such as Finite Element Method (FEM), the results are found to be more realistic and accurate. The FE-Simplorer based co-simulation-based analysis carried out in section-IV-B models both the BLDC motor (FE) and its controller-based drive system (Simplorer), involving huge computational time for analysis. The numerical solutions are based on ordinary and partial differential equations (PDEs) solved with respect to time, t and space x, y, z. The computational time taken is more since the discretization of the absolute space into multiple finite elements is executed which further linearizes to converge the solution for each element. The results thus accomplished are found to be more accurate since the method involves comprehensive analysis of the system. The computational speed is significantly less due to the increase in simulation time.

However, the proposed hybrid fault modeling approach confers complex solutions based on EEC, MEC and NM based techniques. The faults under study, viz. SITF, demagnetization and combined fault effects can be modeled effectively through the hybrid fault model approach. The faults are

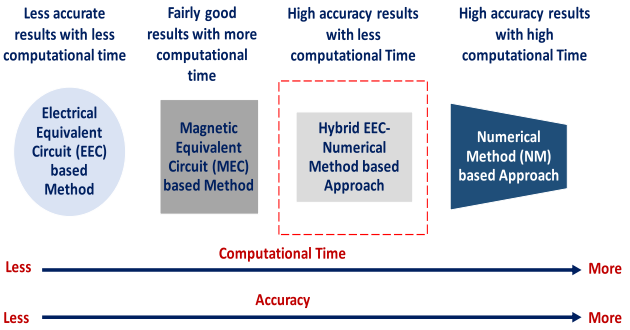

FIGURE 33. Computational time and accuracy-based comparison for different fault modeling methods of BLDC motor.

modeled using the proposed approach in section-IV of this paper, where computational time of modeling was found to be comparatively less than the NM based approach, but higher than the EEC and MEC based methods. It is observed that the computational speed is moderately optimum since the hybrid method involves both the EEC and NM based techniques which are complementary to each other in terms of computational *time* and *speed*. The solutions thus accomplished takes into consideration machine's physical geometry, material properties, non-ideal characteristics like saturation and unequal mutual inductances of the winding respectively. The results are found to be of higher accuracy than the EEC and MEC based approaches consuming less computational time when compared to the NM based techniques. Based on this analysis, an inference is drawn as illustrated in Fig. 33. It is found that as one tends to move from the EEC based methods towards the NMs, the results accomplished are of high accuracy. However, there is an increase in computational time (for a given processor). The proposed hybrid EEC-NM based approach is a middle approach, compromising on the accuracy when compared to NMs and computational time as compared to EEC based methods.

The proposed and validated system thus finds its suitability among efficient and fast modeling techniques for machine fault diagnosis in industrial applications. In addition,

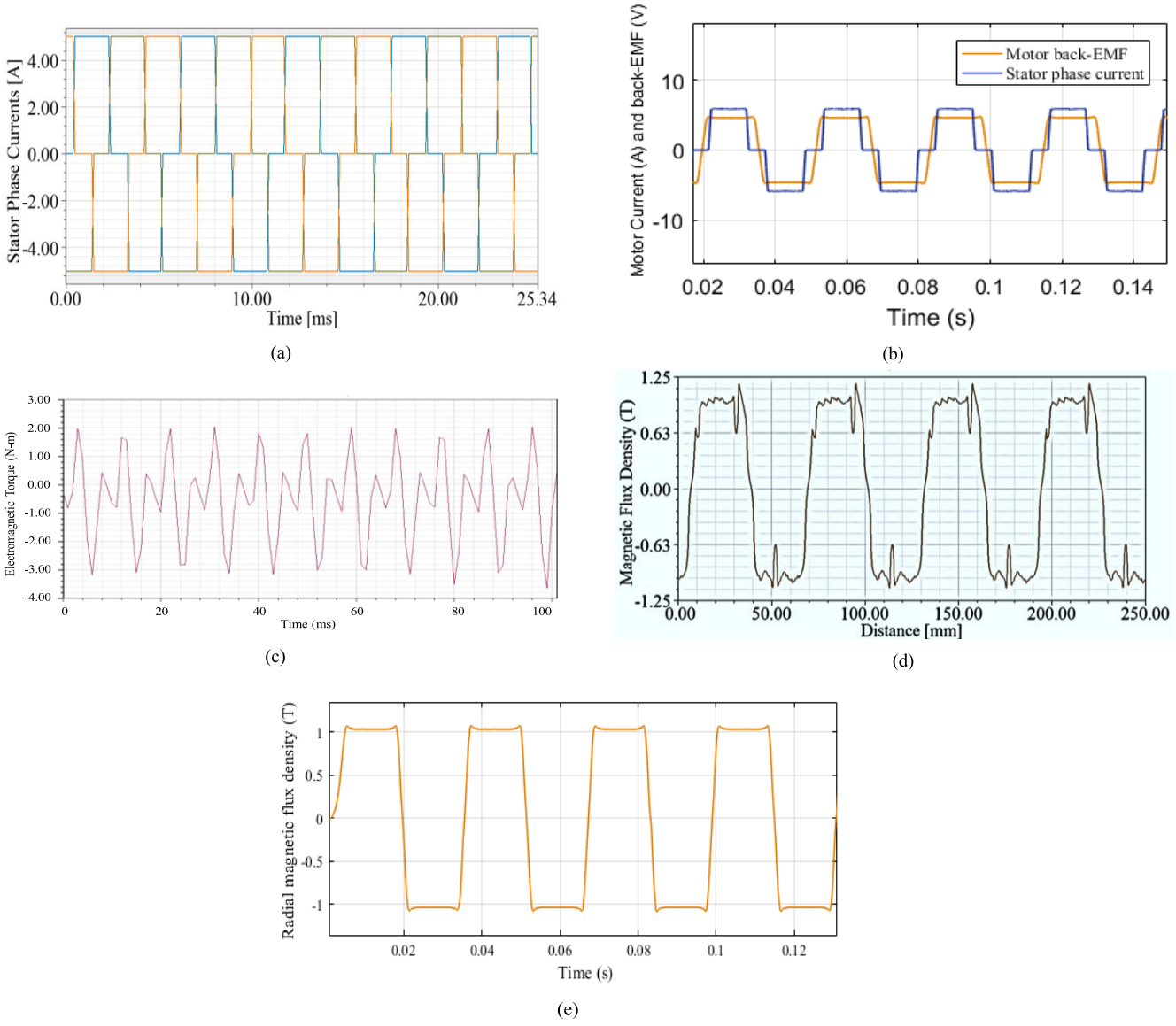

FIGURE 34. (a) The load torque $T_l = 0.5$ N-m is applied to the machine drive under healthy operating conditions. The corresponding stator phase currents is found to be $I_{ph} = 5.8$ A. The torque constant is $K_T = 0.3$ N-m/A (FEA). (b) For a load torque $T_l = 0.5$ N-m applied to the machine drive under healthy operating conditions, the corresponding stator phase currents is found to be I_{ph}5.8 A and the motor back-EMF EB = 5.2 V (Hybrid Model). (c) Electromagnetic torque for the loaded conditions. The $T_l = 0.5$ N-m is applied to the machine. The corresponding average torque inclusive of no-load torque (comprising of windage and frictional losses) is found to be Te = 1.5 N-m. (d) Radial airgap magnetic flux density for loaded conditions. The PM B_g remains the same even during the loaded conditions. B_g is found to be 1.01 T (FEA). (e) Radial airgap magnetic flux density for loaded conditions. The PM B_g remains the same even during the loaded conditions. B_g is found to be 1T (Hybrid Model).

the changes encountered in the electromagnetic quantities of the machine are feasible to model through the hybrid model system which is fast and efficient to detect and diagnose the motor faults. The additional contribution of diagnosing the fault using radial magnetic flux signatures further aids in identifying the fault. The modeling of magnetic flux in the proposed modeling method further gives reliable solutions for machine fault diagnosis. This is justified when the proportional reduction in magnetic flux density is encountered during the demagnetization faults in contrary to the insignificant or unchanged behavior observed in flux for the SITF conditions.

The identification and classification of faults can thus be accomplished through the changes encountered in the characteristic performance of machine quantities. Consequently, based on the type of fault, the required maintenance scheduling can be preponed to avoid prolonged failure of the complete drive system. Based on the research findings and investigations, the BLDC motor fault classification is summarized in Table-7.

IX. BLDC MOTOR PERFORMANCE UNDER LOADED CONDITIONS

In addition to the research work been carried out for a BLDC motor drive under subjected conditions, the performance of the motor is also studied under loaded conditions for both healthy and fault conditions. The rated motor current and electromagnetic torque (T_e) for the machine under study is 21 A and 3.06 N-m respectively (given in Table-1). The torque for the given machine is estimated through the mathematical equations given through (21)-(24). The angular speed ω_m of a rotor is given by (21),

$$\frac{d\omega_m}{dt} = \frac{T_e - T_l}{J} - \frac{B\omega_m}{J} \tag{21}$$

where, T_e is a electrical torque, T_l is a load torque, B is a frictional constant, J is a motor inertia. The electrical torque equation can be given as:

$$Te = \frac{e_a * i_a + e_b * i_b + e_c * i_c}{\omega_m} \tag{22}$$

$$T_e = \frac{P}{2}\frac{e_a i_a + e_b i_b + e_c}{\omega_m} \tag{23}$$

For a square waveform,

$$T_e = \frac{P}{2}\frac{*2 * E_{max} I_{max}}{\omega_m} \tag{24}$$

where P is no. of poles, e_a, e_b, e_c are motor back-EMF of phase A, B and C while i_a, i_b and i_c are stator phase currents of phase A,B and C. The rotor speed is given through ω_m. When a load torque of $T_l = 0.5$ N-m is applied to the motor under healthy operating conditions, the corresponding motor characteristics in terms of electromagnetic quantities are given through Fig. 34. (a)-(c).

The $T_l = 0.5$ N-m when applied to the machine drive under healthy operating conditions, the corresponding stator phase currents is found to be $I_{ph} = 5.8$ A and motor back-EMF is 5.2 V as given in Fig. 34. (a)-(b), operating under 120-degree conduction mode. The machine under investigation has a torque constant of $K_T = 0.3$ N-m/A, corresponding to which, the average torque generated is 1.5 N-m, shown in Fig. 34. (c). The motor is under constant power operation and therefore any change in torque is balanced with the corresponding change in mechanical speed. In addition, there is no change in radial airgap magnetic flux density, since the PM has a constant flux density of $B_g = 1$ T as validated through Fig. 34. (d)-(e). under healthy operating conditions.

However, when a BLDC motor drive under loaded conditions, is subjected to the effect of faults as studied earlier in this paper, the change in electromagnetic quantities are found to be similar. The stator phase current rises due to the applied load and the corresponding generated torque validates (21)-(24). During the SITF conditions the stator phase current rises to significant values (inclusive of load current) as shown through Fig. 35. (a). The corresponding change in electromagnetic torque with ripples induced is given in Fig. 35. (b). As studied earlier that during the SITF conditions there is no significant change in radial magnetic flux density, therefore the similar effect is observed even for the machine under load conditions as shown in Fig. 35. (c). However, the partial decrease in B_g is due to the effect of fault currents (in addition to the load current), initiating partial demagnetization effect within the reversible *BH* characteristic curve as shown in Fig. 11.

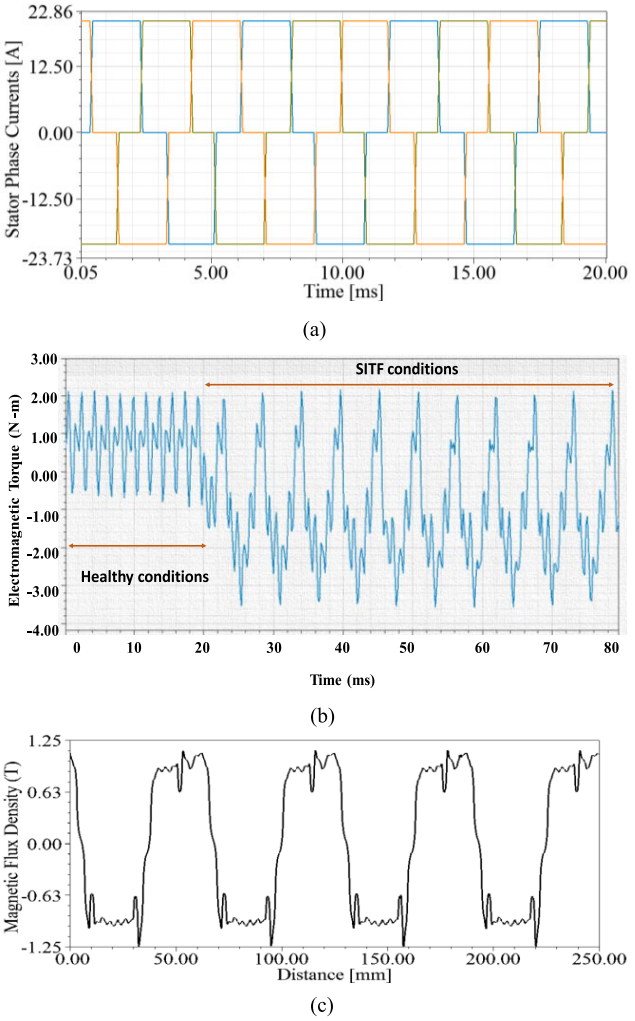

FIGURE 35. (a) The rise in stator phase currents during the SITF conditions which is found to be above 12.5 A. The fault currents are in addition to the load currents since the machine is operating under the loaded conditions. (b) Electromagnetic torque of a machine under load conditions. The corresponding average torque inclusive of no-load torque (comprising of windage and frictional losses) is found to be above 2.5 N-m. The significant torque ripples validate the existence of faults in the machine. (c) There is a marginal change in the radial airgap magnetic flux density for the SITF effects under the loaded conditions. The subjected fault effects under the loaded conditions initiates the partial demagnetizing effect in the rotor PM of a machine within the reversible BH characteristic curve.

Similarly, for a machine drive under loaded conditions, when subjected to demagnetization effects, has an incremental change in electromagnetic torque as shown in Fig. 36. (a) which is due to the increase in stator phase currents. However, the change in radial magnetic flux density remains same and the proportional reduction in the corresponding half cycles validates the demagnetized PMs as shown in Fig. 36. (b).

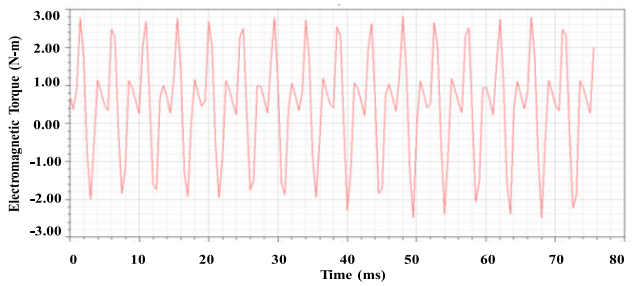

(a)

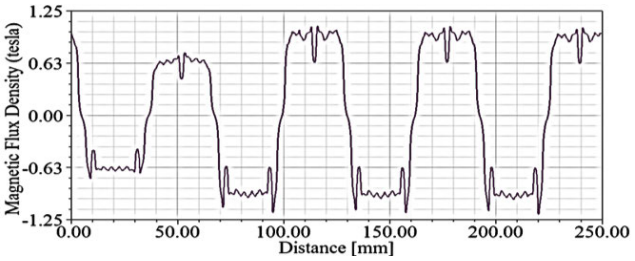

(b)

FIGURE 36. **(a) Electromagnetic torque for the loaded conditions. The corresponding average torque inclusive of no-load torque (comprising of windage and frictional losses) is found to be Te = 2.1 N-m during demagnetization fault effects. The torque ripples are due to the subjected irreversible demagnetization conditions. (b) The reduction in radial airgap magnetic flux density for the corresponding demagnetized PMs. The detrimental characteristic performance of the machine for the demagnetization fault remains the same even for the loaded conditions.**

The study thus reveals that the characteristic change in behavior of machine quantities remains same even under the loaded conditions.

X. CONCLUSION

The proposed research work comprehensively studies the modeling and analysis of Stator Inter-turn Fault (SITF), rotor demagnetization effects and combined effect of both the faults in BLDC motor. The modeling approaches like Electrical Equivalent Circuit (EEC), Improved Winding Function Theory (IWFT), Magnetic Equivalent Circuit (MEC) and Numerical Method (NM) based approaches are used to model the machine effectively. The modeling of stator winding inductance L_S using IWFT and rotor magnetic fields B_g using MEC-NM based approach, are used to develop a novel hybrid model system for diagnosing and classifying the faults. The proposed accuracy-computational time-based analysis further elucidate the effectiveness of the developed modeling approach in giving classification to machine faults.

In addition, the fault investigation and analysis based on the electromagnetic signatures like motor back-EMF and radial magnetic flux density has been the significant contribution of the proposed research work. The distinct and distinguishing characteristics obtained during the existence of both the faults simultaneously, gives identification to the individual faults.

In addition, the proposed method of diagnosing the fault is validated under loaded conditions and therefore find suitability in wide industrial motor drive applications where the highly efficient and fast diagnostic technique is required for diagnosing the motor faults in its incipient stage.

ACKNOWLEDGMENT

The authors would like to thank Ministry of Electronics and Information Technology (MeitY), Government of India for financial support.

REFERENCES

[1] J. R. Hendershot and T. J. E. Miller, *Design of Brushless Permanent Magnet Motors*. New York, NY, USA: Oxford Univ. Press, 1994.
[2] H. Toliyat, S. Nandi, S. Choi, and H. Meshgin-Kelk, *Electric Machines: Modeling, Condition Monitoring, and Fault Diagnosis*. Boca Raton, FL, USA: CRC Press, 2016.
[3] A. Usman, B. M. Joshi, and B. S. Rajpurohit, "Review of fault modeling methods for permanent magnet synchronous motors and their comparison," in *Proc. 11th Int. Symp. Diagnostics Elect. Mach., Power Electron. Drives (SDEMPED)*, Tinos, Greece, Aug./Sep. 2017, pp. 141–146.
[4] S. Nandi and H. A. Toliyat, "Condition monitoring and fault diagnosis of Electrical Machines-A Review," in *Proc. 34th IEEE Ind. Appl. Soc. Annu. Meeting Conf.*, Oct. 1999, pp. 197–204.
[5] J. Faiz and H. Nejadi-Koti, "Demagnetization fault indexes in permanent magnet synchronous motors—An overview," *IEEE Trans. Magn.*, vol. 52, no. 4, pp. 1–11, Apr. 2016.
[6] T. J. E. Miller, M. Popescu, C. Cossar, and M. McGilp, "Performance estimation of interior permanent-magnet brushless motors using the voltage-driven flux-MMF diagram," *IEEE Trans. Magn.*, vol. 42, no. 7, pp. 1867–1872, Jul. 2006.
[7] S. Moon, H. Jeong, H. Lee, and S. W. Kim, "Detection and classification of demagnetization and interturn short faults of IPMSMs," *IEEE Trans. Ind. Electron.*, vol. 64, no. 12, pp. 9433–9441, Dec. 2017.
[8] K.-T. Kim, Y.-S. Lee, and J. Hur, "Transient analysis of irreversible demagnetization of permanent-magnet brushless DC motor with interturn fault under the operating state," *IEEE Trans. Ind. Appl.*, vol. 50, no. 5, pp. 3357–3364, Sep./Oct. 2014.
[9] T. Goktas, M. Zafarani, K. W. Lee, B. Akin, and T. Sculley, "Comprehensive analysis of magnet defect fault monitoring through leakage flux," *IEEE Trans. Magn.*, vol. 53, no. 4, pp. 1–10, Apr. 2017.
[10] Y. Park, D. Fernandez, S. B. Lee, D. Hyun, M. Jeong, S. K. Kommuri, C. Cho, D. D. Reigosa, and F. Briz, "Online detection of rotor eccentricity and demagnetization faults in PMSMs based on Hall-effect field sensor measurements," *IEEE Trans. Ind. Appl.*, vol. 55, no. 3, pp. 2499–2509, May 2019.
[11] M. S. Khan, U. V. Okonkwo, A. Usman, and B. S. Rajpurohit, "Finite element modeling of demagnetization fault in permanent magnet direct current motors," in *Proc. IEEE Power Energy Soc. Gen. Meeting (PESGM)*, Portland, OR, USA, Aug. 2018, pp. 1–5.
[12] O. A. Mohammed, Z. Liu, S. Liu, and N. Y. Abed, "Internal short circuit fault diagnosis for PM machines using FE-based phase variable model and wavelets analysis," *IEEE Trans. Magn.*, vol. 43, no. 4, pp. 1729–1732, Apr. 2007.
[13] M. A. Mazzoletti, G. R. Bossio, C. H. De Angelo, and D. R. Espinoza-Trejo, "A model-based strategy for interturn short-circuit fault diagnosis in PMSM," *IEEE Trans. Ind. Electron.*, vol. 64, no. 9, pp. 7218–7228, Sep. 2017.
[14] Y. Qi, E. Bostanci, M. Zafarani, and B. Akin, "Severity estimation of interturn short circuit fault for PMSM," *IEEE Trans. Ind. Electron.*, vol. 66, no. 9, pp. 7260–7269, Sep. 2019.
[15] N. Leboeuf, T. Boileau, B. Nahid-Mobarakeh, N. Takorabet, F. Meibody-Tabar, and G. Clerc, "Inductance calculations in permanent-magnet motors under fault conditions," *IEEE Trans. Magn.*, vol. 48, no. 10, pp. 2605–2616, Oct. 2012.
[16] T. Kim, H.-W. Lee, and S. Kwak, "The internal fault analysis of brushless DC motors based on the winding function theory," *IEEE Trans. Magn.*, vol. 45, no. 5, pp. 2090–2096, May 2009.
[17] D. Zarko, D. Ban, and T. A. Lipo, "Analytical calculation of magnetic field distribution in the slotted air gap of a surface permanent-magnet motor using complex relative air-gap permeance," *IEEE Trans. Magn.*, vol. 42, no. 7, pp. 1828–1837, Jul. 2006.
[18] N. Bracikowski, M. Hecquet, P. Brochet, and S. V. Shirinskii, "Multiphysics modeling of a permanent magnet synchronous machine by using lumped models," *IEEE Trans. Ind. Electron.*, vol. 59, no. 6, pp. 2426–2437, Jun. 2012.

ADIL USMAN (Senior Member, IEEE) received the B.E. and M.Tech. degrees from Visvesvaraya Technological University (VTU), Belagavi, and the Ph.D. degree from the Indian Institute of Technology Mandi, India. His research interests include fault diagnosis in brushless permanent magnet (PM) synchronous motors, battery management system (BMS) in hybrid electric vehicles (HEVs), and global humanitarian challenges. He is a Life Member of The Institution of Engineers, India. He is an Active Volunteer of IEEE for more than a decade and holds several responsibilities in the capacity of IEEE MGA Student Professional Awareness (SPAx) Chair for Region 1-10. He is currently a Young Professional Representative for Power & Energy Society (PES-YP) from India.

BHARAT SINGH RAJPUROHIT (Senior Member, IEEE) received the M.Tech. degree from the Indian Institute of Technology Roorkee, India, and the Ph.D. degree from the Indian Institute of Technology Kanpur, India. He is currently working as an Associate Professor with the School of Computing and Electrical Engineering, Indian Institute of Technology Mandi, India. His research interests include power electronics and grid integration of renewable energy sources (RES).